

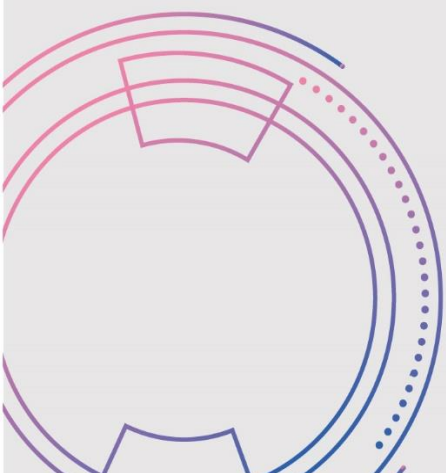


**Firat University  
Journal of Experimental  
and Computational  
Engineering**

Volume: 1

Issues: 3

Year: 2022



**Owner**

On Behalf of Firat University

**Rector**

Prof. Dr. Fahrettin GÖKTAŞ

**Editor-in-Chief**

Prof. Dr. Mehmet YILMAZ, Firat University, Turkey

**Vice Editor-in-Chief**

Prof. Dr. Ebru AKPINAR, Firat University, Turkey

Prof. Dr. Ragıp İNCE, Firat University, Turkey

Prof. Dr. Levent TAŞÇI, Firat University, Turkey

Prof. Dr. Yakup DEMİR, Firat University, Turkey

Prof. Dr. Mete Onur KAMAN, Firat University, Turkey

Assoc. Prof. Dr. Erkut YALÇIN, Firat University, Turkey

**Editorial Advisory Board**

Prof. Dr. Abdulkadir Cüneyt AYDIN, Atatürk University, Turkey

Prof. Dr. Abdussamet ARSLAN, Gazi University, Turkey

Prof. Dr. Ahmet ŞAŞMAZ, Firat University, Turkey

Prof. Dr. Arif GÜLTEN, Firat University, Turkey

Prof. Dr. Baha Vural KÖK, Firat University, Turkey

Prof. Dr. Bilal ALATAŞ, Firat University, Turkey

Prof. Dr. Erhan AKIN, Firat University, Turkey

Prof. Dr. Erkan KÖSE, Nuh Naci Yazgan University, Turkey

Prof. Dr. Filiz KAR, Firat University, Turkey

Prof. Dr. Hasan SOFUOĞLU, Karadeniz Technical University, Turkey

Prof. Dr. İhsan DAĞTEKİN, Firat University, Turkey

Prof. Dr. İsmail Hakkı ALTAŞ, Karadeniz Technical University, Turkey

Prof. Dr. Kazım TÜRK, İnönü University, Turkey

Prof. Dr. M. Şaban TANYILDIZI, Firat University, Turkey

Prof. Dr. Mehmet KARAKÖSE, Firat University, Turkey

Prof. Dr. Mehtap MURATOĞLU, Firat University, Turkey

Prof. Dr. Nevin ÇELİK, Firat University, Turkey

Prof. Dr. Oğuz GÜNGÖR, Ankara University, Turkey

Prof. Dr. Oğuz YAKUT, Firat University, Turkey

Prof. Dr. Özge Kaya HANAY, Firat University, Turkey

Prof. Dr. Paki TURGUT, İnönü University, Turkey

Prof. Dr. Selçuk ÇEBİ, Yıldız Technical University, Turkey

Prof. Dr. Taner ALATAŞ, Firat University, Turkey

Prof. Dr. Yusuf AYVAZ, Yıldız Technical University, Turkey

Assoc. Prof. Dr. Fatih ÖZYURT, Firat University, Turkey

#### Editorial Board

Prof. Dr. Mehmet YILMAZ (Editor-in-Chief)	Civil Engineering
Prof. Dr. Ebru AKPINAR (Vice Editor-in-Chief)	Mechanical Engineering
Prof. Dr. Ragıp İNCE (Vice Editor-in-Chief)	Civil Engineering
Prof. Dr. Levent TAŞÇI (Vice Editor-in-Chief)	Civil Engineering
Prof. Dr. Yakup DEMİR (Vice Editor-in-Chief)	Electrical-Electronics Engineering
Prof. Dr. Mete Onur KAMAN (Vice Editor-in-Chief)	Mechanical Engineering
Assoc. Prof. Dr. Erkut YALÇIN (Vice Editor-in-Chief)	Civil Engineering
Prof. Dr. Abdullah Hilmi LAV	Civil Engineering
Prof. Dr. Ali TOPAL	Civil Engineering
Prof. Dr. Ali YAZICI	Software Engineering
Prof. Dr. Arif GAYDAROV	Chemical Engineering
Prof. Dr. Ayşe Vildan BEŞE	Chemical Engineering
Prof. Dr. Bilge Hilal CADIRCI EFELİ	Bioengineering
Prof. Dr. Ertan EVİN	Mechanical Engineering
Prof. Dr. Evren Meltem TOYGAR	Mechanical Engineering
Prof. Dr. Gülşad Uslu ŞENEL	Environmental Engineering
Prof. Dr. Kadir TURAN	Mechanical Engineering
Prof. Dr. H. Soner ALTUNDOĞAN	Bioengineering
Prof. Dr. Mehmet Deniz TURAN	Metallurgy and Materials Engineering
Prof. Dr. Mehmet YETMEZ	Mechanical Engineering
Prof. Dr. Murat ELİBOL	Bioengineering
Prof. Dr. Mustafa YANALAK	Geodesy and Photog. Engineering
Prof. Dr. Nicola TARQUE	Civil Engineering
Prof. Dr. Nuno MENDES	Mechanical Engineering
Prof. Dr. Rashid NADİROV	Chemical
Prof. Dr. Serdar Ethem HAMAMCI	Electrical-Electronics Engineering
Prof. Dr. Vizureanu PETRICA	Material Processing Technologies
Prof. Dr. VLadimir RYBAKOV	Mathematics and Computer Science
Assoc. Prof. Dr. Alvaro Garcia HERNANDEZ	Civil Engineering
Assoc. Prof. Dr. Baigenzhenov OMİRSERİK	Metallurgical Engineering
Assoc. Prof. Dr. Ebru DURAL	Civil Engineering
Assoc. Prof. Dr. Edip AVŞAR	Environmental Engineering
Assoc. Prof. Dr. Ersin Yener YAZICI	Mining Engineering
Assoc. Prof. Dr. Fatih ÇETİŞLİ	Civil Engineering
Assoc. Prof. Dr. Jülide ÖNER	Civil Engineering
Assoc. Prof. Dr. Marcin SAJDAK	Environmental Engineering and Energy
Assoc. Prof. Dr. Ömer GÖKKUŞ	Environmental Engineering
Assoc. Prof. Dr. Serdar ÇARBAŞ	Civil Engineering
Assoc. Prof. Dr. Tacettin GEÇKİL	Civil Engineering
Assoc. Prof. Dr. Erkut YALÇIN	Civil Engineering
Assist. Prof. Dr. Alvaro Aracena CAIPA	Chemical Engineering
Assist. Prof. Dr. Bahadır YILMAZ	Civil Engineering
Assist. Prof. Dr. Durmuş YARIMPABUÇ	Mathematics
Assist. Prof. Dr. Serap KOÇ	Mechanical Engineering
Assist. Prof. Dr. Ömer Saltuk BÖLÜKBAŞI	Metallurgy and Materials Engineering
Assist. Prof. Dr. Özlem AYDIN	Fod Engineering
Dr. Amilton Barbosa Botelho JUNİOR	Chemical Engineering
Dr. Norman TORO	Metallurgical Engineering
Res. Assist. Dr. Dragana BOZIC	Mining and Metallurgy Institute
Res. Assist. Dr. Jelena MİLOJKOVIĆ	Mineral Raw Materials Tech. Institute
Res. Assist. Dr. Serkan ERDEM	Civil Engineering
Res. Assist. Dr. Ulaş Baran BALOĞLU	Computer Engineering
Res. Assist. Shoeleh ASSEMI	Material Engineering
Lecturer Abdullah Gökhan TUĞAN (Language Editor)	English Language Teaching
Mustafa Gani GENÇER (Language Editor)	English Language Teaching
Res. Assist. Dr. Özge Erdoğan YAMAÇ (Pub. Coordinators)	Civil Engineering
Res. Assist. Beyza Furtana YALÇIN (Secretariat)	Civil Engineering

#### Composition

Hakan YURDAKUL

#### Correspondence Address

Firat University Faculty of Engineering Journal of Experimental and Computational Engineering Publishing Coordinatorship  
23119 Elazığ/TÜRKİYE

E-mail: [fujece@firat.edu.tr](mailto:fujece@firat.edu.tr)

Web page: <http://fujece.firat.edu.tr/>

Firat University Journal of Experimental and Computational Engineering a peer-reviewed journal.

CONTENTS

---

Numerical determination of the production rate and cumulative production in the constant pressure outer boundary condition (Research Article)	
Sabit basınçlı dış sınır şartı durumunda üretim hızının ve kümülatif üretimin sayısal belirlenmesi (Araştırma Makalesi)	
<b>Iredia Davis ERHUNMWUN, Mohammed Idaomi SALIU, Patrick Ejebeare AMIOLEMHEN</b>	<b>94</b>
Investigation of some thermophysical properties of Asphodelus aestivus reinforced polyester composite (Research Article)	
Çiriş otu takviyeli polyester kompozitin bazı termofiziksel özelliklerinin incelenmesi (Araştırma Makalesi)	
<b>Ramazan ORHAN, Ercan AYDOĞMUŞ</b>	<b>103</b>
Determination of water sensitivity of nanosilica added hot mix asphalt (Research Article)	
Nanosilika katkılı sıcak karışım asfaltın suya karşı hassasiyetinin belirlenmesi (Araştırma Makalesi)	
<b>Tacettin GEÇKİL, Ceren Beyza İNCE, Eda Tüzün ÖZPINAR</b>	<b>110</b>
Classification of recyclable waste using deep learning architectures (Research Article)	
Derin öğrenme mimarileri kullanılarak geri dönüştürülebilir atıkların sınıflandırılması (Araştırma Makalesi)	
<b>Arzu SEVİNÇ, Fatih ÖZYURT</b>	<b>122</b>
Failure mechanism of a soil slope and stabilization method: a case study (Case Report)	
Bir zemin şevinin yenilme mekanizması ve stabilizasyon yöntemi: vaka çalışması (Olgu Sunumu)	
<b>Mustafa KANIK</b>	<b>129</b>

---



## Numerical determination of the production rate and cumulative production in the constant pressure outer boundary condition

### Sabit basınçlı dış sınır şartı durumunda üretim hızının ve kümülatif üretimin sayısal belirlenmesi

Iredia Davis ERHUNMWUN<sup>1\*</sup>, Mohammed Idaomi SALIU<sup>2</sup> and Patrick Ejebeheare AMIOLEMHEN<sup>3</sup>

<sup>1,2,3</sup> Department of Production Engineering, Faculty of Engineering, University of Benin, Benin City, Nigeria.

<sup>1</sup>iredia.erhunmwun@uniben.edu, <sup>2</sup>mohammed\_saliu@yahoo.com, <sup>3</sup>patrick.amiolemhen@uniben.edu

Received: 17.05.2022

Revision: 16.06.2022

doi: 10.5505/fujece.2022.77487

Accepted: 21.07.2022

Research Article

#### Abstract

The flow regime is identified as a steady-state flow if the pressure at every location in the reservoir remains constant. In this work, we have determined the well production rate and cumulative production in a circular reservoir using the Finite Element Method for the condition of constant pressure outer boundary. The reservoir was divided into 4 smaller part known as finite element. These parts were analyzed and later assembled to form the domain of the reservoir. The analysis was done with the assumption that before the well begins production, there was uniform distribution of pressure all through the reservoir. The results obtained from the production rate analysis shows that the dimensionless production rate decreases significantly and later becomes uniform because the withdrawn fluid has been completely replaced. This condition remains throughout the entire life of the reservoir presumably. Also, the result shows that there is a uniform increase in the dimensionless cumulative production as time increases. The result obtained in this work was compared with the results obtained by previous researcher. The comparison shows a strong positive correlation between the two methods with a maximum percentage error of 0.1711 and 0.1864 and a minimum percentage error of 0.0001 and 0.0122 for dimensionless production rate and dimensionless cumulative production respectively. Also, result from previous researcher only state the production rate and cumulative production of the reservoir at a particular time but this work predicts the production rate and cumulative production in the entire reservoir at the same time.

**Keywords:** Diffusivity equation, Boundary condition, Cumulative production, Production rate, Finite element method.

#### Özet

Rezervuarın her noktasındaki basınç sabit kalırsa, akış rejimi kararlı durum akışı olarak tanımlanır. Bu çalışmada, dairesel bir rezervuarda kuyu üretim hızı ve kümülatif üretim, sabit basınç dış sınır koşulu için Sonlu Elemanlar Metodu kullanılarak belirlendi. Rezervuar, sonlu eleman olarak bilinen 4 küçük parçaya bölünmüştür. Bu parçalar analiz edildi ve daha sonra rezervuarın alanını oluşturmak için birleştirildi. Analiz, kuyu üretime başlamadan önce, tüm rezervuar boyunca eşit basınç dağılımı olduğu varsayımıyla yapıldı. Üretim hızı analizinden elde edilen sonuçlar, boyutsuz üretim hızının önemli ölçüde azaldığını ve daha sonra çekilen sıvı tamamen değiştirildiği için üniform hale geldiğini göstermektedir. Bu durum muhtemelen rezervuarın tüm ömrü boyunca devam eder. Ayrıca sonuç, zaman arttıkça rezervuardaki boyutsuz kümülatif üretimde tek tip bir artış olduğunu göstermektedir. Bu çalışmada elde edilen sonuç, Christine tarafından elde edilen sonuçlarla karşılaştırıldı. Karşılaştırma, boyutsuz üretim hızı ve boyutsuz kümülatif üretim için sırasıyla 0.1711 ve 0.1864 maksimum yüzde hatası ve 0.0001 ve 0.0122 minimum yüzde hatası ile iki yöntem arasında güçlü bir pozitif korelasyon gösterir. Ayrıca Christine çözümleri, yalnızca belirli bir zamanda rezervuarın üretim hızını ve kümülatif üretimini belirtir, ancak bu çalışma aynı anda tüm rezervuardaki üretim hızını ve kümülatif üretimi tahmin eder.

**Anahtar kelimeler:** Yayılma denklemi, Sınır koşulu, Birikimli üretim, Üretim hızı, Sonlu elemanlar yöntemi.

#### 1. Introduction

The finite element technique has over the years been so well established that today it's seems to be one of the best methods for analysing the efficiency of a wide variety of practical problems. In fact, the method has become one of the research areas for applied mathematicians [1]. The basic idea in the finite element method is actually to find the

\*Corresponding author

solution of a complicated problem by replacing it with a simpler one [2]. For many years now, the finite element method has been considered to be a numerical, and mathematically well defined, discretization method for simulating and analysing a wide variety of boundary value problems. Finally, the finite element method is a very versatile method and has found applications in many engineering problems. Today, there are over 100000 engineers that make use of the finite element method [3].

The semi-analytical techniques that have found wide application in researches in fluid dynamics were the similarity approach, the perturbation methods, and the integral methods (all for the viscous boundary layer calculations) and the methods of characteristics (for inviscid compressible flow simulations) [4]. The fluid flow in reservoir or in porous medium has been a great interest of physicists, engineers and hydrologists who tried to predict the behaviours of compressible and incompressible fluids. They have designed several experiments so as to validate the implementation of their proposed correlations [5]. The basic equation for predicting pressure distribution in a reservoir is the diffusivity equation. Several methods have proposed to solve the diffusivity equation including numerical and analytical approaches.

The diffusivity equation has been solved in dimensionless form [6]. Chakrabarty with some other researchers provided a quantitative analysis of the effects of neglecting the quadratic gradient term on solving the diffusion equation governing the transient state [7]. It should be noted that among the flow regimes in reservoir, the transient flow was the most significant state upon which such important characteristics such as permeability, reservoir capacity, and skin factor can be determined using well test analysis [6], [8]. Barreto and Peres developed a nonlinear hydraulic diffusivity equation that governs the flow of compressible fluids in porous media. In their study, a general solution that properly accounts for both fluid property behaviour and variable rate was presented. The proposed solution, which was derived from the Green's-function method by recasting the effect of the viscosity-compressibility product variation as a nonlinear source term, can handle variable gas rate for several well-reservoir geometries of practical interest [9].

Couto and Marsili presented the application of the integral transform technique in the development of a general analytical solution for the multidimensional hydraulic diffusivity equation. The solution methodology dealt directly with time-dependent well rates and boundary conditions, sparing the use of the superposition principle [10]. Wu and Li generalized mathematical framework model and numerical approach for unconventional-gas-reservoir simulation. The model and numerical scheme were based on generalized flow models with unstructured grids [11].

In the analysis of the diffusivity equation, large computation times occur because the solution involves the infinite series. Each term of the series requires evaluation of exponentials and Bessel functions and the series itself was sometimes slowly convergent and that inaccuracies can result from lack of computer precision or from the use of improper methods of numerical computation [12]. Therefore, they presented a computationally efficient and accurate new methodology in differential quadrature analysis of diffusivity equation to overcome these difficulties. The methodology would overcome the difficulties in boundary conditions implementations of second order partial differential equations encountered in such problems. A new mathematical technique called the Homotopy Analysis Method (HAM) has been used to solve the radial diffusivity equation for slightly compressible fluid [12].

A comparison between analytical and numerical solution for both linear and nonlinear diffusivity equation has been performed at wellbore radius, and secondly, a comprehensive sensitivity analysis was done to find the significant physical properties of reservoir which influence the pressure drop. Also a comprehensive analysis of parameters such as depletion time, reservoir radius and production rate to find where the pressure differences of linear and non-linear diffusivity equations were significant [13].

In all the literature reviewed so far, none of the methods has been able to look holistically at the dimensionless cumulative production and production rate in the constant pressure outer boundary condition using the finite element method, hence, the need for this work.



## 2. Methodology

The diffusivity equation can be used to determine the flow properties in a circular reservoir. This equation is as shown in eq. (1) below.

$$\frac{\partial^2 P_D}{\partial r_D^2} + \frac{1}{r_D} \frac{\partial P_D}{\partial r_D} = \frac{\partial P_D}{\partial t_D} \quad (1)$$

and the initial and boundary conditions become:

1. Dimensionless initial condition:

$$\text{Uniform pressure in the reservoir } P_D(r_D, t_D = 0) = 0 \quad (2)$$

2. Dimensionless Inner Boundary Condition:

$$\text{Constant rate at the well } \frac{\partial P_D}{\partial r_D}(1, t_D) = 1 \quad (3)$$

3. Dimensionless Outer Boundary Conditions:

- a. "Infinite Acting" Reservoirs

$$\text{No reservoir boundary } P_D(r_D \rightarrow \infty, t_D) = 0 \quad (4)$$

- b. "No Flow" boundary:

$$\text{No flux across the reservoir } \frac{\partial P_D}{\partial r_D}(r_{eD}, t_D) = 0 \quad (5)$$

- c. Constant Pressure Boundary:

$$\text{Constant pressure outer boundary } P_D(r_{eD}, t_D) = 0 \quad (6)$$

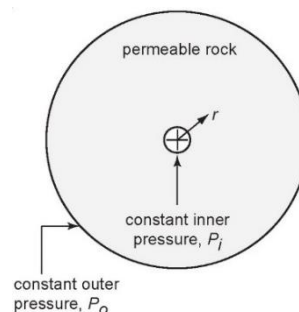


**Figure 1.** Constant pressure outer boundary

Eq. (1) can also be written in a condensed form as:

$$\frac{1}{r_D} \frac{\partial}{\partial r_D} \left( r_D \frac{\partial P_D}{\partial r_D} \right) = \frac{\partial P_D}{\partial t_D} \quad (7)$$

In the analysis involving Finite Element method, the governing equation can only be solved if it is in order one. But the governing equation for the diffusivity equation is in order two, so, the need to weaken the governing equation to order one. This is followed by the introduction of the interpolation functions to enable us derive the finite element model. This model is used to generate the elemental matrices and finally assembled to represent the entire domain of the reservoir. The assembled matrix cannot be solved directly. But with the introduction of either the boundary condition or initial conditions or a combination of both the initial and boundary conditions, the nodal values of the parameter can be determined. These procedures were followed and eq. (7) becomes:

$$[K_{ij}^e] \{P_D\} + [M_{ij}^e] \left\{ \dot{P}_{Dj} \right\} = \{Q_i^e\} \quad (8)$$

Eq. 8 is the developed finite element model of the diffusivity equation under the unsteady state flow regime.

$$\text{where } K_{ij}^e = \int_{r_{DA}}^{r_{DB}} r_D \frac{d\psi_i^e}{dr_D} \frac{d\psi_j^e}{dr_D} dr_D \quad (9)$$

$$M_{ij}^e = \int_{r_{DA}}^{r_{DB}} r_D \psi_i^e \psi_j^e dr_D \quad (10)$$

Using Quadratic Lagrange Interpolation functions for a quadratic element:

$$\psi_1(r_D) = \frac{1}{h_e^2} (h_e + r_{DA} - r_D)(h_e - 2r_D + 2r_{DA}) \quad (11)$$

$$\psi_2(r_D) = \frac{4}{h_e^2} (r_D - r_{DA})(h_e + r_{DA} - r_D) \quad (12)$$

$$\psi_3(r_D) = \frac{-1}{h_e^2} (r_D - r_{DA})(h_e - 2r_D + 2r_{DA}) \quad (13)$$

## 2.1. Time approximation

Since the problem is a time dependent problem, we convert the ordinary differential equation in time to algebraic equation and the most commonly used method is the  $\alpha$  family of interpolation. In doing this, a weighted average of the time derivative of the dependent variable is approximated to two consecutive time steps by linear interpolation of the values of the variables of the two steps.

For a given time step  $s$ , eq. (8) becomes

$$[K_{ij}^e] \{P_D\}_s + [M_{ij}^e] \left\{ \dot{P}_{Dj} \right\}_s = \{Q_i^e\}_s \quad (14)$$

For the next time step  $s+1$ , eq. (8) becomes



$$[K_{ij}^e] \{P_D\}_{s+1} + [M_{ij}^e] \left\{ \dot{P}_{Dj} \right\}_{s+1} = \{Q_i^e\}_{s+1} \quad (15)$$

Multiply eq. (14) by  $(1-\alpha)$  and eq. (15) by  $\alpha$ , then we add the two resulting equations, we have

$$[M_{ij}^e] \left[ (1-\alpha) \left\{ \dot{P}_{Dj} \right\}_s + \alpha \left\{ \dot{P}_{Dj} \right\}_{s+1} \right] + [K_{ij}^e] \left[ (1-\alpha) \{P_{Dj}\}_s + \alpha \{P_{Dj}\}_{s+1} \right] = (1-\alpha) \{Q_i^e\}_s + \alpha \{Q_i^e\}_{s+1} \quad (16)$$

The  $\alpha$  family of interpolation for time consideration is given as:

$$(1-\alpha) \left\{ \dot{P}_{Dj} \right\}_s + \alpha \left\{ \dot{P}_{Dj} \right\}_{s+1} = \frac{\{P_{Dj}\}_{s+1} - \{P_{Dj}\}_s}{\Delta t_{s+1}} \quad (17)$$

Substitute eq. (17) into eq. (16) and using the Crank-Nicholson Scheme where  $\alpha = 1/2$ ,

$$\left[ [M_{ij}^e] + \frac{\Delta t_{s+1}}{2} [K_{ij}^e] \right] \{P_{Dj}\}_{s+1} = \left[ [M_{ij}^e] - \frac{\Delta t_{s+1}}{2} [K_{ij}^e] \right] \{P_{Dj}\}_s + \frac{\Delta t_{s+1}}{2} [\{Q_i^e\}_s + \{Q_i^e\}_{s+1}] \quad (18)$$

Substituting the initial condition, we have:

$$\left\{ \bar{Q}_i^e \right\} = \left[ \frac{1}{\Delta t_1} [M_{ij}^e] + \frac{1}{2} [K_{ij}^e] \right] \{P_{Dj}\}_1 - \left[ \frac{1}{\Delta t_1} [M_{ij}^e] - \frac{1}{2} [K_{ij}^e] \right] \{P_{Dj}\}_0 \quad (19)$$

### 3. Results and Discussion

The flow regime is identified as a steady-state flow if the pressure at every location in the reservoir remains constant, i.e., does not change with time. Mathematically, this condition is expressed as:

$$P = P_e = \text{Constant at } r = r_e, \text{ i.e., } P_D(r_D \rightarrow r_{eD}, t_D) = 0 \text{ and } \frac{\partial P}{\partial t} = 0 \quad \forall \text{ r and t} \quad (20)$$

This equation states that the rate of change of pressure  $p$  with respect to time  $t$  at any location  $i$  is zero. In reservoirs, the steady-state flow condition can only occur when the reservoir is completely recharged and supported by strong aquifer or pressure maintenance operations, i.e. this condition is appropriate when pressure is being maintained in the reservoir due to either natural water influx or artificially by the injection of some displacing fluid. The pressure can also be maintained as a result of gas cap expansion support.

The semi-steady state flow equations are frequently applied when the rate, and consequently the position of the closed boundary surrounding a well, is slowly varying functions of time. If the production rate of an individual well is changed, for instance, due to closure for repair or increasing the rate to obtain a more even fluid withdrawal pattern throughout the reservoir, there will be a brief period when transient flow conditions prevail followed by stabilized flow for the new distribution of individual well rates.

Thus, this solution of the diffusivity equation models radial flow of slightly compressible liquid in a homogeneous reservoir of uniform thickness; reservoir at uniform pressure before production; unchanging pressure at the outer boundary; and production at constant rate from a single well (centred in the reservoir) with wellbore radius.

The results obtained from this analysis were shown in the form of graphs of dimensionless production rate. These were shown in Figs. 2 to 7. These were shown for different dimensionless radii ranging between 100 and 1000000. It was seen from the graph that the dimensionless production rate history of the reservoir was not captured at the initial stage between the dimensionless time of zero and the respective dimensionless times in Figs. 2 and 7. This was due to the fact that, within these regions, the reservoir was still at the infinite acting region. After the infinite acting period, it was observed that the dimensionless production rate decreases significantly and later becomes uniform because the withdrawn fluid has been completely replaced. This condition remains throughout the entire life of the reservoir presumably.

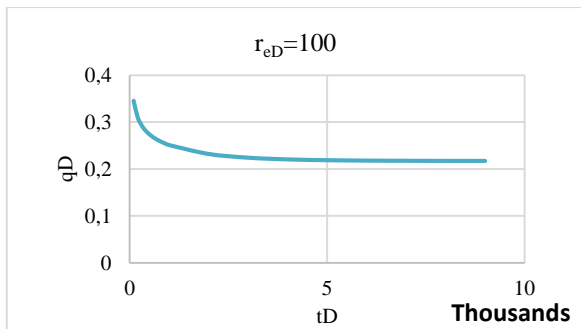


**Figure 2.** A graph of  $q_D$  against  $t_D$  at  $r_{eD}=100$

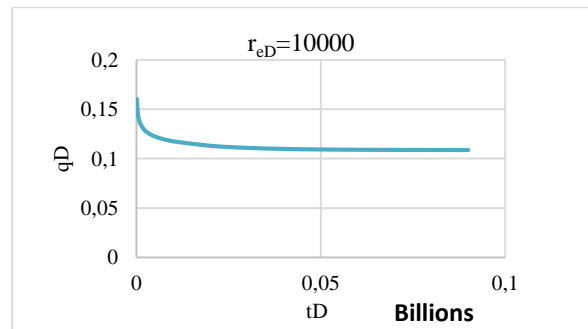


**Figure 5.** A graph of  $q_D$  against  $t_D$  at  $r_{eD}=10000$

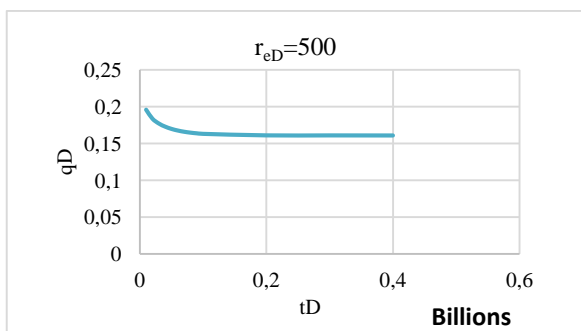


**Figure 3.** A graph of  $q_D$  against  $t_D$  at  $r_{eD}=500$

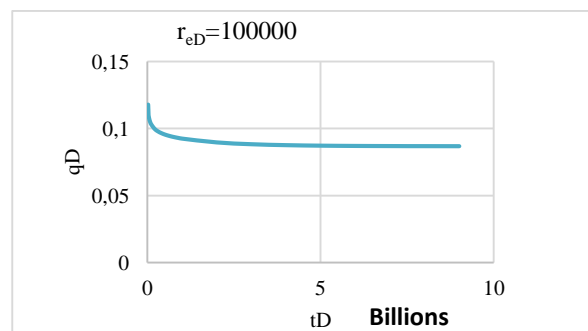


**Figure 6.** A graph of  $q_D$  against  $t_D$  at  $r_{eD}=100000$

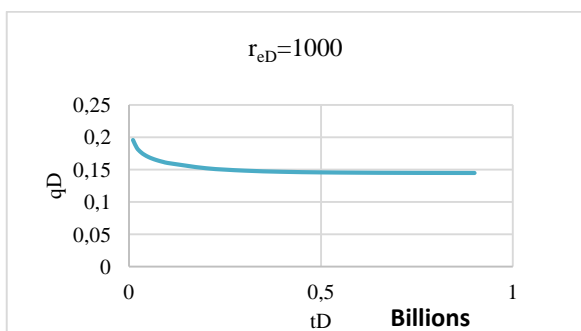


**Figure 4.** A graph of  $q_D$  against  $t_D$  at  $r_{eD}=1000$

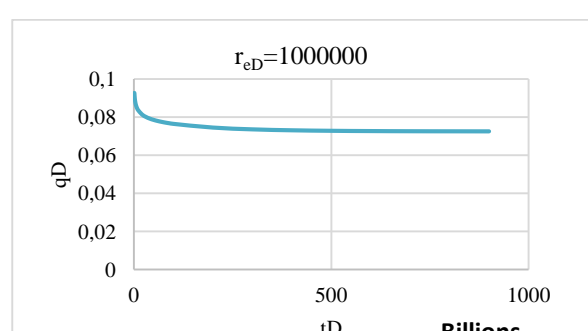


**Figure 7.** A graph of  $q_D$  against  $t_D$  at  $r_{eD}=1000000$

Also in this study, the results obtained from this analysis were shown in the form of graphs of dimensionless cumulative production against dimensionless time. These were shown in Figures 8 to 13. These were shown for different dimensionless radii ranging between 20 and 1000000. It was seen from the graph that the dimensionless cumulative production history of the reservoir was not captured at the initial stage between the dimensionless time of zero and the respective dimensionless times in Figures 8 and 13. This was due to the fact that, within these regions,

the reservoir was still at the infinite acting region. After the infinite acting period, it was observed that the dimensionless production rate increases uniformly throughout the entire life of the reservoir.

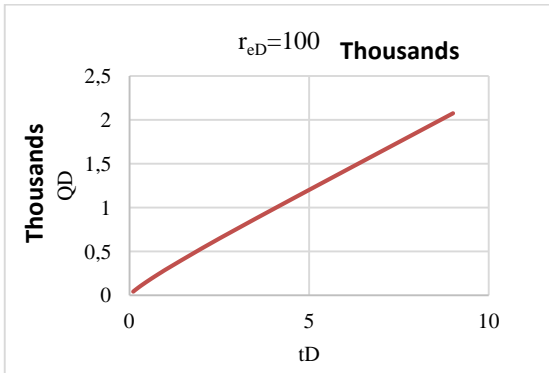


Figure 8. A graph of  $Q_D$  against  $t_D$  at  $r_{eD}=100$

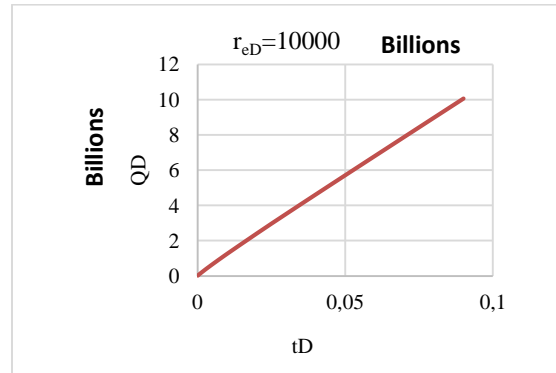


Figure 11. A graph of  $Q_D$  against  $t_D$  at  $r_{eD}=10000$

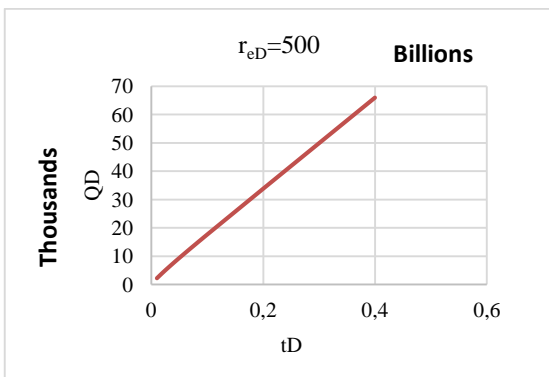


Figure 9. A graph of  $Q_D$  against  $t_D$  at  $r_{eD}=500$

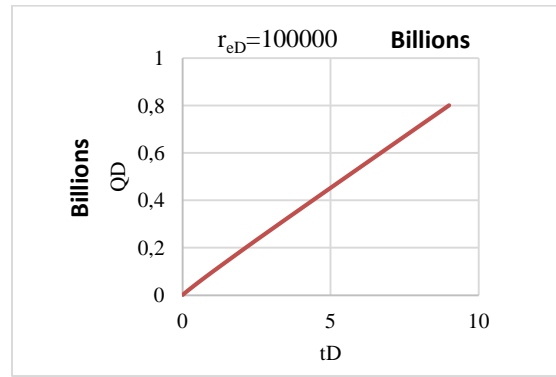


Figure 12. A graph of  $Q_D$  against  $t_D$  at  $r_{eD}=100000$

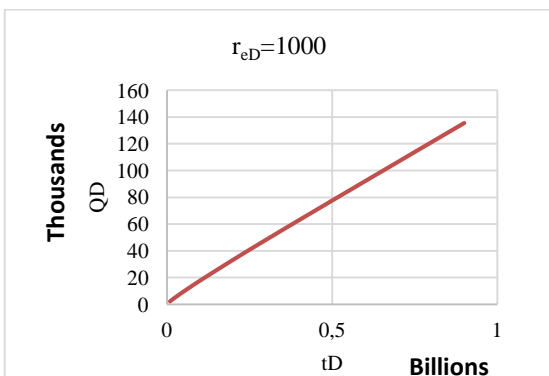


Figure 10. A graph of  $Q_D$  against  $t_D$  at  $r_{eD}=1000$

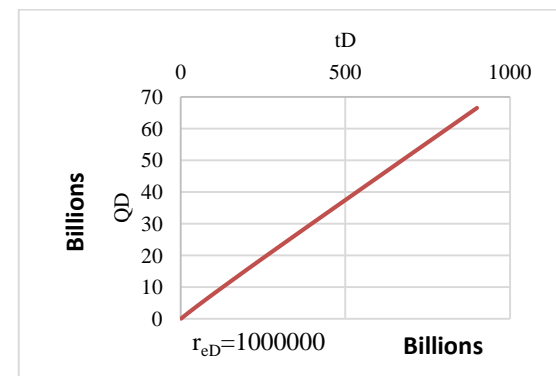


Figure 13. A graph of  $Q_D$  against  $t_D$  at  $r_{eD}=1000000$

The accuracy of the results was also obtained by computing a table of percentage errors. Table 1 shows the percentage error between the finite element method solutions and Christine [14]. The results show the level of discrepancies between the two results. It was shown that there was a strong agreement between the two results.

**Table 1.** Percentage error between this work and Christine [14] result at various dimensionless time and radii (100-10000)

$t_D$	$r_{eD}=100$		$r_{eD}=500$		$r_{eD}=1000$		$r_{eD}=10000$				
	$Q_D$ % error	$q_D$ % error	$t_D$	$Q_D$ % error	$q_D$ % error	$t_D$	$Q_D$ % error	$q_D$ % error	$t_D$	$Q_D$ % error	$q_D$ % error
100	0.0033	0.0413	10000	0.0650	0.0729	10000	0.0204	0.0729	100000	0.0813	0.0891
200	0.0019	0.0460	20000	0.0349	0.0778	20000	0.0204	0.0778	200000	0.0431	0.0940
300	0.0014	0.0487	30000	0.0242	0.0806	30000	0.0204	0.0806	300000	0.0297	0.0968
400	0.0011	0.0507	40000	0.0187	0.0826	40000	0.0204	0.0826	400000	0.0228	0.0989
500	0.0009	0.0522	50000	0.0153	0.0841	50000	0.0204	0.0842	500000	0.0185	0.1004
600	0.0008	0.0534	60000	0.0129	0.0852	60000	0.0204	0.0855	600000	0.0157	0.1017
700	0.0007	0.0545	70000	0.0112	0.0861	70000	0.0204	0.0866	700000	0.0136	0.1028
800	0.0006	0.0554	80000	0.0099	0.0867	80000	0.0204	0.0875	800000	0.0120	0.1038
900	0.0005	0.0562	90000	0.0089	0.0872	90000	0.0204	0.0883	900000	0.0108	0.1046
1000	0.0005	0.0569	100000	0.0081	0.0876	100000	0.0204	0.0891	1000000	0.0098	0.1053
2000	0.0003	0.0616	200000	0.0042	0.0887	200000	0.0204	0.0939	2000000	0.0051	0.1103
3000	0.0002	0.0638	300000	0.0029	0.0887	300000	0.0204	0.0962	3000000	0.0035	0.1131
4000	0.0001	0.0648	400000	0.0022	0.0888	400000	0.0204	0.0974	4000000	0.0027	0.1152

**Table 2.** Percentage error between this work and Christine [14] result at various dimensionless time and radii (50000-1000000)

$r_{eD}=100000$			$r_{eD}=1000000$			$r_{eD}=50000$		
$t_D$	$Q_D$ % error	$q_D$ % error	$t_D$	$Q_D$ % error	$q_D$ % error	$t_D$	$Q_D$ % error	$q_D$ % error
10000000	0.1711	0.0122	1000000000	0.0022	0.1544	10000000	0.1711	0.1217
20000000	0.0892	0.0121	2000000000	0.0011	0.1593	20000000	0.0892	0.1275
30000000	0.0609	0.0129	3000000000	0.0008	0.1622	30000000	0.0609	0.1295
40000000	0.0465	0.0132	4000000000	0.0006	0.1642	40000000	0.0465	0.1315
50000000	0.0377	0.0133	5000000000	0.0005	0.1658	50000000	0.0377	0.1331
60000000	0.0317	0.0134	6000000000	0.0004	0.1671	60000000	0.0317	0.1344
70000000	0.0274	0.0135	7000000000	0.0003	0.1682	70000000	0.0274	0.1355
80000000	0.0242	0.0136	8000000000	0.0003	0.1692	80000000	0.0242	0.1364
90000000	0.0216	0.0137	9000000000	0.0003	0.1700	90000000	0.0216	0.1373
100000000	0.0196	0.0138	10000000000	0.0002	0.1708	100000000	0.0196	0.1380
200000000	0.0102	0.0143	20000000000	0.0013	0.1757	200000000	0.0102	0.1429
300000000	0.0069	0.0146	30000000000	0.0009	0.1786	300000000	0.0069	0.1458
400000000	0.0053	0.0148	40000000000	0.0006	0.1806	400000000	0.0053	0.1479
500000000	0.0043	0.0149	50000000000	0.0005	0.1822	500000000	0.0043	0.1494
600000000	0.0036	0.0151	60000000000	0.0004	0.1835	600000000	0.0036	0.1506
700000000	0.0031	0.0152	70000000000	0.0004	0.1846	700000000	0.0031	0.1514
800000000	0.0027	0.0153	80000000000	0.0003	0.1856	800000000	0.0027	0.1521
900000000	0.0024	0.0154	90000000000	0.0003	0.1864	900000000	0.0024	0.1527

#### 4. Conclusion

In this research, we have formulated the finite element base models for the diffusivity equation under the steady state flow regime. The result obtained where used to analyse the production rate and cumulative production for different

radii and time. In the constant pressure outer boundary condition where the pressure at the external boundary of the reservoir was held constant because the reservoir was been recharged by a very strong aquifer.

The accuracy of the results has been validated by comparing the results with existing results in literature. The result from this research shows a strong positive correlation between the results with existing results in literature. Finally, the accuracy of the results obtained was admissible and it therefore shows that the Finite element method can be used in approximating the dimensionless production rate and cumulative production values of fluid in circular reservoirs.

## 5. Acknowledgements

We want to acknowledge the Department of Production Engineering, University of Benin, Nigeria for serving as a platform to embark on this research.

## 6. Author Contribution Statement

All the authors in this research made on or two contributions towards the success of this research. Author 1, provided the finite element solution of the diffusivity equation while Author 2 used the result from the first author to analyze the reservoir production rate and cumulative production. Author 3 supervised the research and help in the validation of the result using relevant literature.

## 7. Ethics Committee Approval and Conflict of Interest

There is no need for an ethics committee approval in the prepared article and there is no conflict of interest with any person/institution in the prepared article.

## 8. References

- [1] Rao SS. *The Finite Element Method in Engineering*, 2<sup>nd</sup> ed. Pergamon Press, Oxford, U.K. 1982.
- [2] Rao SS. *Finite Element Method in Engineering*. 2<sup>nd</sup> and 3<sup>rd</sup> ed. 1992.
- [3] Zienkiewicz OC. *The Finite Element Method*, 5th ed. (volume 1) The Basic, 2000.
- [4] Van Dyke M. *Perturbation Methods in Fluid Mechanics*. Academic Press, 1964.
- [5] Ahmed T and McKinney P. *Advanced reservoir engineering*. Gulf Professional Publishing, Oxford, 2011.
- [6] Lee WJ. Pressure transient testing part 9. *Production engineering methods*. In: Development Geology Reference Manual. AAPG Methods in Exploration No. 10, Tulsa, OK, 477-481, 1992.
- [7] Chakrabarty C, Ali S, Tortike W. "Analytical solutions for radial pressure distribution including the effects of the quadratic gradient term". *Water Resour Res*, 29(4), 1171-1177, 1993.
- [8] Van Everdingen A. "The skin effect and its influence on the productive capacity of a well". *J Petrol Techn.*, 5(06), 171-176, 1953.
- [9] Barreto AB, Peres AM. "A variable-rate solution to the nonlinear diffusivity gas equation by use of green's-function method". *SPE Journal*, 145468, 2012.
- [10] Couto P, Marsili MD. "A general analytic solution for the multidimensional hydraulic diffusivity equation by integral transform technique". *Rio de Janeiro, Brazil, OTC*, 29-31, 2013.
- [11] Wu YS, Li J. "A generalised framework model for the simulation of gas production in unconventional gas reservoirs". *SPE Journal*, 163609, 2014.
- [12] Folade OA, Chukwunagolu VS. "Homotopy Analysis Solution to Radial Diffusivity Equation of Slightly Compressible Fluid". *Appl. Maths.*, 7(9), 93-1004, 2016.
- [13] Reza A, Mohamad M, Zahra S. "Parametric analysis of diffusivity equation in oil reservoirs". *J Petrol Explor Prod Technol*, 6, 1-11, 2016.
- [14] Christine, AE. Well test analysis for wells produced at constant pressure. PhD thesis submitted to the Department of Petroleum Engineering and the Committee on Graduate Studies of Stanford University, 1979.



## Investigation of some thermophysical properties of *Asphodelus aestivus* reinforced polyester composite

### Çiriş otu takviyeli polyester kompozitin bazı termofiziksel özelliklerinin incelenmesi

Ramazan ORHAN<sup>1</sup> , Ercan AYDOĞMUŞ<sup>2\*</sup> 

<sup>1,2</sup>Department of Chemical Engineering, Faculty of Engineering, Firat University, Elazığ, Türkiye.

<sup>1</sup>[rorhan@firat.edu.tr](mailto:rorhan@firat.edu.tr), <sup>2</sup>[ercanaydogmus@firat.edu.tr](mailto:ercanaydogmus@firat.edu.tr)

Received: 21.07.2022

Accepted: 04.08.2022

Revision: 02.08.2022

doi: 10.5505/fujece.2022.66375

Research Article

#### Abstract

In this research, both environmentally friendly and economical composites have been produced by using biomass wastes in unsaturated polyester. The use of renewable biomass wastes as a filler in unsaturated polyester is reduced the carbon footprint of the composite obtained. A low-density and flexible structure could be achieved according to the intended use of polyester composites. While the density of the pure polyester polymer not reinforced with biomass is around 1206 kg/m<sup>3</sup>, the density of the 5 wt.% filler added composite decreases to 1167 kg/m<sup>3</sup>. Biomass waste (*Asphodelus aestivus* L.) reduces Shore D hardness of the polyester composite and turns it into a more flexible and easy-to-process material. It has been observed that the thermal conductivity coefficient of the biomass reinforced polyester composite shows a slight increase compared to the pure polyester composite. Besides, it has been determined that as the amount of biomass in the polyester composite increases, the activation energy decreases. The specific bond structure in the polyester polymer has been determined by Fourier transform infrared (FTIR) spectroscopy. Biomass waste is not making a chemical bond with polyester, it is only used as a filler. Also, the surface morphology of the polyester composite has been investigated with the help of scanning electron microscopy (SEM). The use of 3 wt.% *Asphodelus aestivus* L. biomass as a filler does not create a negative pore structure on the composite surface.

**Keywords:** Polyester composite, Biomass, Density, Hardness, Thermal conductivity, Activation energy.

#### Özet

Bu araştırmada biyokütle atıkları doymamış polyester içerisinde kullanılarak hem çevre dostu hem de ekonomik kompozitler üretilmektedir. Yenilenebilir biyokütle atıklarının doymamış polyesterde dolgu maddesi olarak kullanılması, elde edilen kompozitin karbon ayak izini azaltmaktadır. Polyester kompozitlerin kullanım amacına göre düşük yoğunluklu ve esnek bir yapı elde edilebilmektedir. Biyokütle takviye edilmeyen saf polyester polimerin yoğunluğu 1206 kg/m<sup>3</sup> civarında iken, ağırlıkça % 5 dolgu katkılı kompozitin yoğunluğu 1167 kg/m<sup>3</sup>'e düşmektedir. Biyokütle atığı (*Asphodelus aestivus* L.), polyester kompozitin Shore D sertliğini azaltmakta ve onu daha esnek ve işlenmesi kolay bir malzemeye dönüştürmektedir. Biyokütle takviye edilen polyester kompozitin ısı iletkenlik katsayısının saf polyestere göre hafif bir artış gösterdiği gözlemlenmektedir. Ayrıca polyester kompozitteki biyokütle miktarı arttıkça aktivasyon enerjisinin azaldığı tespit edilmektedir. Polyester polimerdeki spesifik bağ yapısı, Fourier transform kızılötesi (FTIR) spektroskopisi ile belirlenmiştir. Biyokütle atığı polyesterde kimyasal bağ yapmamakta, sadece dolgu maddesi olarak kullanılmaktadır. Ayrıca taramalı elektron mikroskobu (SEM) yardımıyla polyester kompozitin yüzey morfolojisi incelenmiştir. Ağırlıkça % 3 *Asphodelus aestivus* L. biyokütlesinin dolgu maddesi olarak kullanılması kompozit yüzeyde negatif gözenek yapısı oluşturmamaktadır.

**Anahtar kelimeler:** Polyester kompozit, Yoğunluk, Sertlik, Termal iletkenlik, Aktivasyon enerjisi.

#### 1. Introduction

In recent years, the application areas of polyester composites have become quite widespread. However, due to the petrochemical composition of such polymers, there is an increasing trend towards alternative biomass sources both in terms of environmental pollution and for economical production. Polyester composite should have some thermophysical

\*Corresponding author

properties such as density, hardness, thermal conductivity, and thermal stability suitable for its intended use. For this purpose, many additives and fillers are used in the production of polyester composites in the literature.

For example, polyester composite has been reinforced with borax as a filler. The use of borax in certain proportions by mass increases the density, hardness, mechanical strength, and thermal stability of the composite [1]. Especially sustainable resources (modified palm oil) and recycled polymers (PET) are also used in the production of polyester composites. Thanks to such additives and fillers, fewer petrochemical components are used and environmentally friendly composites can be improved [2]. Besides, many inorganic fillers are used for the thermal stability of polyester composites at high temperatures. In particular, fillers such as fumed silica (aerosil), colemanite, ulexite, and tincal increase the high-temperature performance of polyester composites [3,9].

In another research in the literature, new biocomposite materials have been developed by making a chemical bond with modified palm oil and modified castor oil. In such studies, both physical and chemical modifications are made to the polyester composite. In this way, low density, porous, flexible, economical, and environmentally friendly composites have been improved [4,5].

In particular, materials such as waste masks and waste polyurethane, which are less recyclable, are used in polyester composites after they are prepared in laboratory conditions and ground to the appropriate particle size. In this way, polyester composite materials with high porosity, low density, and thermal conductivity coefficient can be developed. [6,7].

Also, graphene (GF), silicon carbide (SiC), and multi-walled carbon nanotube (MWCNT) have been used in the production of the polyester nanocomposite. With the help of nanoparticles used in certain proportions, the mechanical strength and thermal stability of the composites increase. By using such nanoparticles, polyester composites with high density and hardness can be obtained [8].

Moreover, organic compounds and inorganic alumina particles synthesized in nano size are also reinforced into the polyester composite. In particular, alumina increases both the mechanical strength and thermal stability of the polyester composite [10]. Moreover, biomass wastes from sustainable sources are also preferred as fillers in polyester composites. Apricot stone shells reduce the density of the polyester composite, improve its mechanical properties, and increase its porosity and surface hardness [11].

The original aspect of this research is the use of a local plant species, *Asphodelus aestivus L.*, as a filler in the polyester composite. In this way, economical, environmentally friendly, and low-density composite materials are obtained with biomass wastes. The density of the produced composite has been evaluated by examining its thermal conductivity coefficient, Shore D hardness, activation energy, chemical bond structure, surface morphology, and porosity.

## 2. Materials and Methods

### 2.1. Materials

In this study, unsaturated polyester (UP), methyl ethyl ketone peroxide (MEKP), and cobalt octoate (Co Oc) were supplied from Turkuaz Polyester Company. Local plant leaves as a filler (*Asphodelus aestivus L.*) were collected and washed in Elazığ (Türkiye) province. After the leaves dried at room temperature and were ground, they were prepared for polyester composite production. The leaves of *Asphodelus aestivus L.* and its powder form after drying and grinding are shown in Figure 1.





Figure 1. *Asphodelus aestivus L.* used as a filler in the production of polyester composite

## 2.2. Experimental method

Biomass is mixed homogeneously into the unsaturated polyester resin as a filler at 0 wt.%, 1 wt.%, 1.5 wt.%, 3 wt.%, and 5 wt.%. Then, certain amounts of MEKP and Co Oc components are added to the mixture, respectively, mixed at 1000 rpm for 2 minutes, and poured into standard molds. After waiting 24 hours for the curing process, necessary testing and analysis processes are carried out. Density, Shore D hardness, activation energy, thermal conductivity coefficient, chemical bond structure, and surface morphology of the obtained polyester composite are investigated. In Table 1, the amounts of the components used in the experimental studies for the production of polyester composites are expressed. Also, the polyester composite production scheme is briefly shown in Figure 2.

Table 1. Polyester composite preparation plan

UP (g)	MEKP (g)	Co Oc (g)	Filler (g)
9.80	0.15	0.05	0.00
9.70	0.15	0.05	0.10
9.65	0.15	0.05	0.15
9.50	0.15	0.05	0.30
9.30	0.15	0.05	0.50

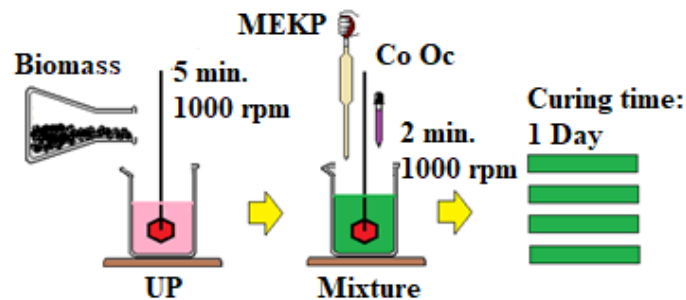


Figure 2. Polyester composite production process and flow chart

## 3. Results and Discussions

### 3.1. Density of polyester composites

After the prepared polyester composites are poured into standard molds, the volume of the matrix formed is calculated. Then, the mass is found and divided by the volume and the density values are calculated. As seen in

Figure 3, it has been determined that the density values of the polyester composite decrease with the filler reinforcement.

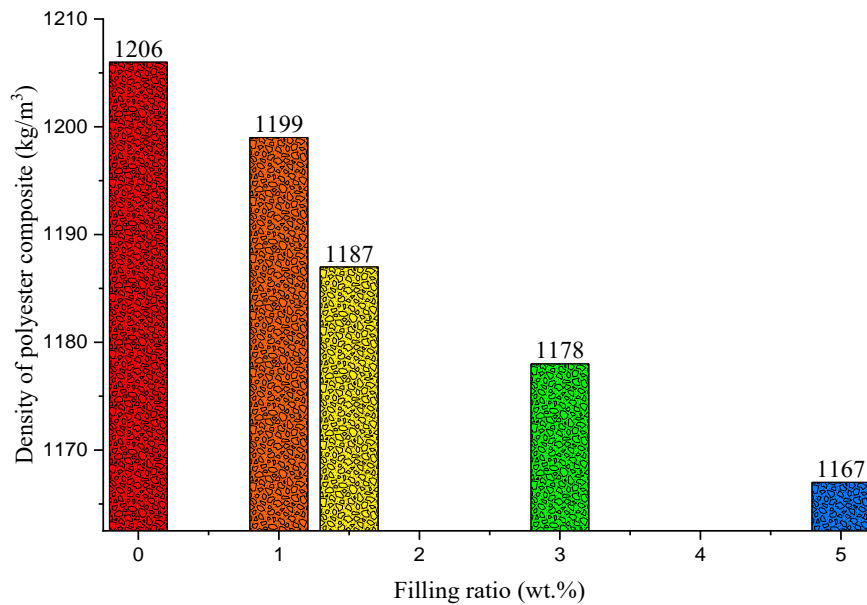


Figure 3. Effect of *Asphodelus aestivus L.* reinforcement on the density of polyester composite

### 3.2. Shore D hardness of polyester composites

Shore D hardness values of polyester composites produced by reinforcement *Asphodelus aestivus L.* are given in Figure 4. As seen in the graph, it has been determined that the filler added to the pure polyester reduces the hardness of the composite sample. While the hardness value for pure polyester is 78 Shore D, it is observed that 5 wt.% filler reinforcement decreases Shore D hardness of the composite to 76.1. In this case, it can be said that cellulosic biomass creates a more flexible structure than pure polyester.

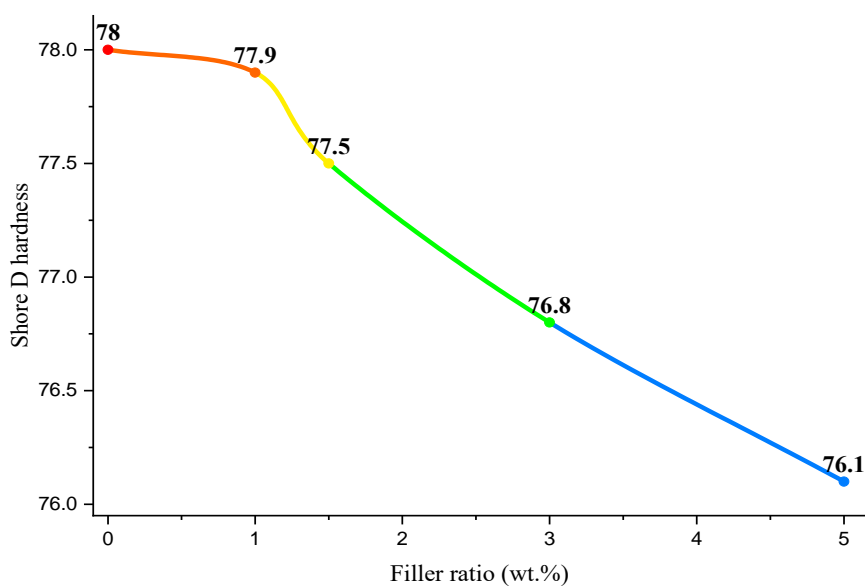
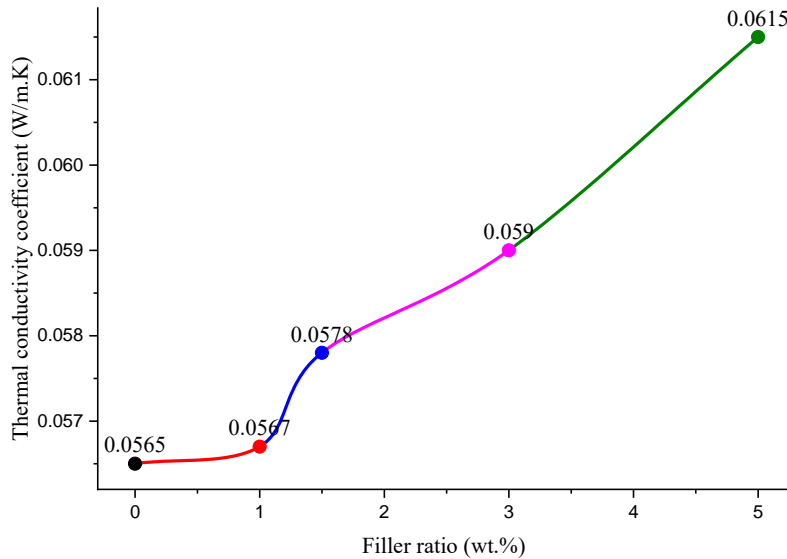


Figure 4. Effect of *Asphodelus aestivus L.* reinforcement on Shore D hardness of polyester composite

### 3.3. Thermal conductivity of polyester composites

In experimental studies, the thermal conductivity coefficient values of polyester composite samples produced using *Asphodelus aestivus L.* are measured using a thermal conductivity meter (Thermtest portable TLS 100). As seen in Figure 5, while the thermal conductivity coefficient of pure polyester is 0.0565 W/m·K, this value increases slightly with the addition of biomass to pure polyester.



**Figure 5.** Effect of *Asphodelus aestivus L.* reinforcement on thermal conductivity of polyester composite

The thermal stability of polyester composites has been evaluated by calculating the activation energies. For this purpose, the weight loss of the prepared samples has been found by measuring the temperature increase and the weight loss in an inert environment in the PID-controlled experiment system. In this study, it has been determined that biomass wastes decrease the activation energy values of the polyester composite. Activation energy ( $E_a$ ) values are calculated according to Coats-Redfern method. In this method, the highest correlation coefficients are obtained with the three-dimensional diffusion equation. Activation energies (conversion ratio: 0.2-0.8) of pure polyester and polyester composites reinforced with the filler are calculated in thermal decomposition experiments that have been carried out at a heating rate of about 10 °C/min to 600 °C. Calculated activation energy values are given in Table 2.

**Table 2.** Calculated  $E_a$  of biomass reinforced composites

Filler ratio (wt.%)	$E_a$ (kJ/mol)
0	114.53
1	108.25
3	104.70
5	102.56

### 3.4. FTIR spectra of polyester composite

In this study, there is no chemical bonding as the leaves of *Asphodelus aestivus L.* plant are used as filler in the polyester composite. Since there is only a physical interaction, there is no difference in FTIR spectra of pure polyester polymer and composite. Figure 6 shows 1240-1100  $\text{cm}^{-1}$  C-O ester groups, 3000  $\text{cm}^{-1}$  C-H bonds, 2900-2850  $\text{cm}^{-1}$   $\text{CH}_2$  groups vibration stresses in FTIR spectra. A peak is observed in the polyester composite at 1720  $\text{cm}^{-1}$  due to the stretching vibrations of the C=O group. The peaks at 1400 and 1450  $\text{cm}^{-1}$  observed in the polyester composite spectrum indicate the aromatic ring. The peak at 1260  $\text{cm}^{-1}$  seen in the polyester spectra is due to the twisting vibration

of the CH<sub>2</sub> groups [6-10].

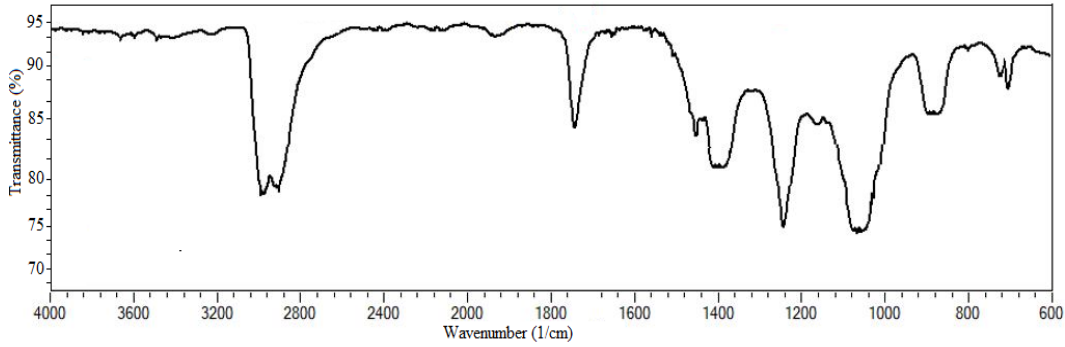


Figure 6. FTIR spectra of polyester composite

### 3.5. SEM image of polyurethane

In Figure 7, an SEM image of the composite is given when the leaves of *Asphodelus aestivus L.* plant are reinforced with polyester at a rate of 3 wt.%. Since the high rate of biomass reinforcement creates an irregular pore structure in the polyester composite, a rate of 3 wt.% has been preferred.

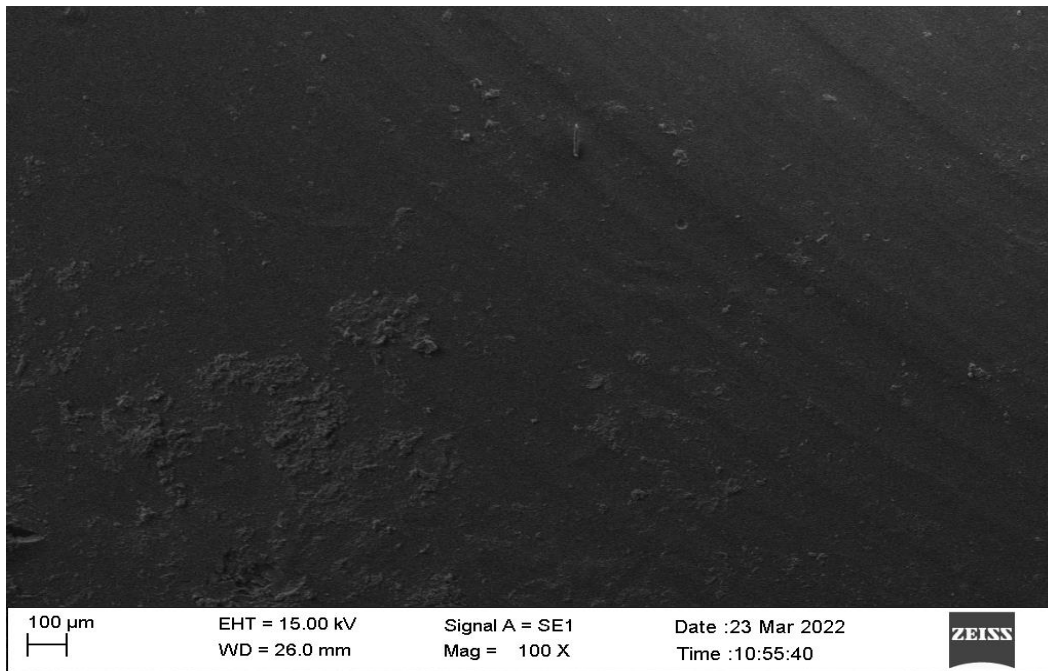


Figure 7. SEM image of *Asphodelus aestivus L.* (3 wt.%) reinforced polyester composite

## 4. Conclusions

In this study, biomass wastes (*Asphodelus aestivus L.*) have been evaluated and both renewable resources are used and economical biomaterials are produced. 1 wt.%, 1.5 wt.%, 3 wt.%, and 5 wt.% biomass waste is reinforced with unsaturated polyester as a filler. Polyester composite materials have been obtained by using the hand casting method under laboratory conditions. Some physical and chemical properties of the produced polyester composite materials are characterized. For example, thermal conductivity coefficient, activation energy, density and hardness, surface morphology, and chemical bond structure of the composites have been evaluated.

According to the results obtained, it has been determined that the density of the biomass reinforced composites decreases. It has been observed that the thermal conductivity coefficient of the polyester composite raises with the increase in biomass in the mixture, albeit slightly. The activation energy of the biomass reinforced polyester composite decreases as the filler increases. Besides, it is determined that Shore D hardness decreases as the amount of filler in the mixture raises.

The use of biomass wastes in the production of composite materials will enable economical composites to be obtained and the development of environmentally friendly biomaterials with a low carbon footprint.

## 5. Acknowledgments

We would like to thank Rama ELCEDAN, an undergraduate student of the Department of Chemical Engineering, who contributed to the experimental studies in the laboratory conditions.

## 6. Author Contribution Statement

Author 1 contributed to making the design, and the literature review contributed to forming the idea, and the analysis of the results. Author 2 contributed to conducting experimental studies, writing the article checking the spelling, and checking in terms of content.

## 7. Ethics Committee Approval and Conflict of Interest

There is no need for an ethics committee approval in the prepared article. There is no conflict of interest with any person/institution in the prepared article.

## 8. References




- [1] Orhan R, Aydoğmuş E, Topuz S, Arslanoğlu H. "Investigation of thermo-mechanical characteristics of borax reinforced polyester composites". *Journal of Building Engineering*. 42, 103051, 2021.
- [2] Aydoğmuş E, Arslanoğlu H, Dağ M. "Production of waste polyethylene terephthalate reinforced biocomposite with RSM design and evaluation of thermophysical properties by ANN". *Journal of Building Engineering*, 44, 103337, 2021.
- [3] Aydoğmuş E, Arslanoğlu H. "Kinetics of thermal decomposition of the polyester nanocomposites". *Petroleum Science and Technology*, 39(13–14), 484–500, 2021.
- [4] Aydoğmuş E. "Biohybrid nanocomposite production and characterization by RSM investigation of thermal decomposition kinetics with ANN". *Biomass Conversion and Biorefinery*, 2022.
- [5] Aydoğmuş E, Dağ M, Yalçın Z G, Arslanoğlu H. "Synthesis and characterization of waste polyethylene reinforced modified castor oil-based polyester biocomposite". *Journal of Applied Polymer Science*, 139, e525256, 2022.
- [6] Demirel MH, Aydoğmuş E. "Production and Characterization of Waste Mask Reinforced Polyester Composite". *Journal of Inonu University Health Services Vocational School*. 10(1), 41-49, 2022.
- [7] Demirel MH, Aydoğmuş E. "Waste Polyurethane Reinforced Polyester Composite, Production and Characterization". *Journal of the Turkish Chemical Society Section A: Chemistry*. 9(1), 443–452, 2022.
- [8] Yanen C, Aydoğmuş E. "Characterization of Thermo-Physical Properties of Nanoparticle Reinforced the Polyester Nanocomposite". *Dicle University Journal of the Institute of Natural and Applied Science*. 10(2), 121–132, 2021.
- [9] Yanen C, Dağ M, Aydoğmuş E. "Investigation of Thermophysical Properties of Colemanite, Ulexite, and Tincal Reinforced Polyester Composites". *European Journal of Science and Technology*, 36, 155–159, 2022.
- [10] Şahal H, Aydoğmuş E. "Investigation of Thermophysical Properties of Polyester Composites Produced with Synthesized MSG and Nano-Alumina". *European Journal of Science and Technology*, 34, 95-99, 2022.
- [11] Orhan R, Topuz S, Aydoğmuş E. "Experimental and Theoretical Study on Mechanical Properties of Apricot Stone Shell Reinforced Polyester Composites". 3. *Asia Pacific International Congress on Contemporary Studies*, South Korea, 2020.





## Determination of water sensitivity of nanosilica added hot mix asphalt

### Nanosilika katkılı sıcak karışım asfaltın suya karşı hassasiyetinin belirlenmesi

Tacettin GEÇKİL<sup>1</sup> , Ceren Beyza İNCE<sup>2\*</sup> , Eda Tüzün ÖZPINAR<sup>3</sup> 

<sup>1,2,3</sup>Department of Civil Engineering, Faculty of Engineering, Inonu University, Malatya, Türkiye.

<sup>1</sup>tacettin.geckil@inonu.edu.tr, <sup>2</sup>c.beyzaince@gmail.com, <sup>3</sup>tuzun\_eda@hotmail.com

Received: 23.06.2022

Accepted: 11.09.2022

Revision: 15.08. 2022

doi: 10.5505/fujece.2022.77486

Research Article

#### Abstract

In this study, the effects of nanosilica (NS) additive on the water sensitivity of hot mix asphalt (HMA) pavements were investigated. For this, NS-modified asphalts were prepared by adding NS at rates of 1%, 3%, 5% and 7% by weight to the pure B 160/220 asphalt. In the study, first of all, the physical properties of pure and modified asphalts were determined by penetration, ductility and softening point experiments, and their viscosities were determined by rotational viscometer (RV) experiment. Then, the optimum asphalt content of the mix was determined according to the Marshall design method. Hot mix asphalt specimens were prepared by keeping this determined ratio constant for pure and modified asphalts. Prepared pure and NS added modified mixture specimens were subjected to Marshall stability, retained Marshall stability (RMS) and indirect tensile strength (ITS) tests. The physical test results showed that the hardness and machinability temperatures of the modified binders increased up to 5% NS. According to the mixture test results, it was determined that NS additive had a positive effect on the sensitivity of road pavements to water, since Marshall stability, RMS and indirect tensile strength ratio (ITSR) values showed significant increases at 5% NS.

**Keywords:** Asphalt, Nanosilica, Hot mix asphalt, Retained marshall stability, ITS.

#### Özet

Bu çalışmada, nanosilika (NS) katkısının sıcak karışım asfalt (HMA) kaplamaların suya karşı hassasiyeti üzerindeki etkileri araştırılmıştır. Bu amaçla, saf B 160/220 asfalta ağırlıkça %1, %3, %5 ve %7 oranlarında NS eklenerek NS modifiyeli asfaltlar hazırlanmıştır. Çalışmada öncelikle saf ve modifiye asfaltların fiziksel özellikleri penetrasyon, düktilite ve yumuşama noktası deneyleri ile viskoziteleri ise dönel viskozimetre (RV) deneyi ile belirlenmiştir. Daha sonra Marshall tasarım yöntemine göre karışımın optimum asfalt içeriği belirlenmiştir. Belirlenen bu oran saf ve modifiye asfaltlar için sabit tutularak sıcak karışım asfalt numuneleri hazırlanmıştır. Hazırlanmış olan saf ve NS katkılı modifiye karışım numuneleri Marshall stabilitesi, kalıcı Marshall stabilitesi (RMS) ve dolaylı çekme mukavemeti (ITS) deneylerine tabi tutulmuştur. Fiziksel test sonuçları, modifiye bağlayıcıların sertlik ve işlenebilirlik sıcaklıklarının %5 NS'ye kadar arttığını göstermiştir. Karışım test sonuçlarına göre, Marshall stabilitesi, RMS ve dolaylı çekme mukavemeti oranı (ITSR) değerlerinin yine %5 NS miktarında önemli artışlar göstermesi sebebiyle, yol kaplamalarının suya karşı hassasiyeti üzerinde NS katkısının olumlu bir etkisi olduğu tespit edilmiştir.

**Anahtar kelimeler:** Asfalt, Nanosilika, Sıcak karışım asfalt, Kalıcı marshall stabilitesi, ITS.

## 1. Introduction

Various environmental factors (temperature, water, etc.) and traffic loads are the two main causes of deteriorations in hot mix asphalt (HMA) pavements. Deteriorations in the pavements (rutting, cracks, water-induced deteriorations, etc.) decrease the pavement performance, reduce the service life of the pavement and minimize driving comfort [1,2].

The service life, durability and performance of the pavement mainly depend on how well the asphalt can bond and adhere to the aggregate surface under different conditions [3]. The water on the pavement leaks into the mixture, causing the bond between asphalt and aggregate to weaken, and this is called "loss of adhesion". The loss of adhesion causes the HMA

\*Corresponding author

pavement to loosen and soften, which is expressed as "segregation" or "loss of cohesion" of the materials in the mixture. When the pavement is exposed to water, important problems occur in the chemical structure of both the asphalt and the aggregate, and as a result, the asphalt begins to decompose from the aggregate. In short, it is possible to state that the deformation caused by water in the HMA pavement is directly related to the loss of adhesion and cohesion [3-5]. In other words, the water in the pavement weakens the adhesion by entering between the asphalt and the aggregate and adversely affects the cohesion by causing decomposition in the structure of the mixture. This causes the pavement to deteriorate. On the other hand, other environmental factors such as the construction of the pavement and the design of the hot mix (air gap percentage, asphalt film thickness, etc.), high temperature, age of the pavement, freeze-thaw cycles, and the properties of the additives in the mixture are also important factors affecting water damage [1, 2, 6].

In order to reduce the deformations caused by water in pavements, silane additives, especially hydrated lime, portland cement, surface agent additives and various traditional liquid additives are used [2,6]. It has been seen in many studies that lime reacts with the structure and strengthens the bond between asphalt and aggregate, especially as a result of adding lime to HMA [2,5,7,8]. However, in recent years, various polymers have also been used in hot mixes to reduce water-induced deteriorations. In many studies, it has been stated that the use of some polymers in asphalt modification, albeit limited, functions as anti-stripping additives [2,9,10]. In addition, the use of various nano-sized materials such as nanosilica in asphalt modification has also been started recently.

Nanosilica is a white crystalline material that is abundant on Earth, in nanometer size and has the chemical formula  $\text{SiO}_2$ . Compared to other nanomaterials, nanosilica is among the most advantageous nanomaterials due to its lower production cost and higher performance properties [3,11]. This material, which has a large surface area, good dispersion ability and adsorption, has superior properties such as good strength and thermal stability at high temperatures. In addition, nanosilica is a frequently used material to produce silica gel, silica gas and similar materials [3,12].

When the studies using nanosilica additive in asphalt modification were examined, it was stated that nanosilica increased the viscosity, softening point and elasticity modulus of asphalt, while decreasing its consistency and ductility [12-14]. In other studies, it was stated that the rheological properties of nanosilica-modified binders improved and their temperature sensitivity decreased [13, 15]. In another study, it was stated that the fatigue life of nanosilica-modified asphalts increased more than nanocalcium carbonate and nanotitanium, and adding 4% nanosilica to asphalt increased the fatigue life of asphalt [16]. It has been observed that the thermal properties of hot mix asphalts are significantly improved with the use of nanosilica additive in HMA mixtures, thus the stiffness modulus of the mixtures increases and the nanosilica increases its resistance to the loads on the HMA pavement [14]. In some studies, it has been observed that the additive of nanosilica retards the oxidation of the asphalt mixture, increasing its stability against moisture damage, and increasing the anti-peeling properties of the mixture, resulting in longer fatigue life and high permanent deformation resistance of the pavement [17-20].

In the current studies carried out so far, it is seen that the nanosilica additive is mostly used in asphalt modification and the physical and rheological properties of asphalt are investigated. In other studies, the properties of nanosilica added mixtures such as fatigue, permanent deformation and fracture resistance were investigated.

In this study, unlike previous studies, the effect of nanosilica additive on the water sensitivity of HMA pavements was investigated. In the study, the effects of nanosilica additive on the resistance of HMA pavements to the harmful effects of water were tried to be determined by Marshall stability, RMS and ITS experiments.

## **2. Materials and Method**

### **2.1. Materials**

In the study, three kinds of materials were used, which are pure asphalt with penetration class B 160/220, nanosilica (NS) additive and crushed limestone aggregate.



The physical properties of asphalt supplied from Turkish Petroleum Refineries Inc. (TUPRAŞ) are given in Table 1. Nanosilica additive (Figure 1) was obtained from Elkem Silicone Material factory and its properties are given in Table 2. The physical properties of the crushed limestone aggregate used for the HMA pavement design are given in Table 3 and its gradation is given in Table 4.

**Table 1.** Properties of asphalt

Properties	Standard	Limit	Result
Penetration (0.1mm)	ASTM D5	160-220	163
Softening point (°C)	ASTM D36	35-43	41.6
Ductility (cm)	ASTM D113	min. 100	125
Flash point (°C)	ASTM D92	min. 220	244
Specific weight (g/cm <sup>3</sup> )	ASTM D70	1.0-1.1	1.038
Penetration index (PI)	-	-	-0.27
Mass loss (%)	ASTM D2872	max. 1.0	0.47



**Figure 1.** Nanosilica additive

**Table 2.** Properties of nanosilica

Properties	NS
Form	Ultrafine amorphous powder
Odor	Odorless
Melting point (°C)	1550-1570
Solubility (Water)	Insoluble/Slightly soluble
Solubility (Organic Solvents)	Insoluble/Slightly Soluble
Density (g/cm <sup>3</sup> )	2.2-2.3
Particle size (nm)	11-13
Surface area (m <sup>2</sup> /g)	200

**Table 3.** Physical properties of aggregate

Properties	Standard	Limit	Result
Coarse aggregate apparent specific gravity (g/cm <sup>3</sup> )	ASTM C127	-	2.711
Coarse aggregate volume specific gravity (g/cm <sup>3</sup> )		-	2.648
Coarse aggregate water absorption (%)		max.2	0.88
Fine aggregate apparent specific gravity (g/cm <sup>3</sup> )	ASTM C128	-	2.750
Fine aggregate volume specific gravity (g/cm <sup>3</sup> )		-	2.664
Fine aggregate water absorption (%)		max.2	1.17
Filler apparent specific gravity (g/cm <sup>3</sup> )	ASTM D 854	-	2.751
Abrasion loss, Los Angeles (%)	ASTM C131	max.30	28
Frost loss (%)	ASTM C88	max.10	4.5
Flat and long grains (%)	ASTM D4791	max.10	4

**Table 4.** Aggregate gradation

Sieve (mm)	19	12.5	9.5	4.75	2.36	1.18	0.6	0.3	0.15	0.075
Passing (%)	100	94	84	58	35	22	16	12	8	5

## 2.2. Method

### 2.2.1. Preparation of NS added asphalt binders

In the study, pure asphalt was first heated up to 150°C. Then, by adding 1, 3, 5 and 7 wt% nanosilica to the asphalt, the resulting blends were mixed with a mixer at 1200 rpm for 60 minutes at the same temperature, and modified asphalts were prepared.

In the study, pure and nanosilica-modified asphalts were coded as P, P+1NS, P+3NS, P+5NS and P+7NS, respectively.

The physical properties of the pure and modified asphalts obtained were determined by conventional tests, and the workability properties were determined by the RV test. All the results obtained are given in Table 5.

**Table 5.** Test results

Properties	Binder types				
	P	P+1NS	P+3NS	P+5NS	P+7NS
Penetration (0.1mm)	163	134	129	124	146
Softening point (°C)	41.6	42.8	44.8	45.1	42.6
Ductility (cm)	125	117	113	109	115
PI	-0.27	-0.57	-0.05	-0.004	-0.32
Mass loss (%)	0.47	0.08	0.10	0.15	0.06
Viscosity (135°C)	287.5	320.0	330.0	350.0	320.0
Viscosity (165°C)	100.0	115.0	135.0	150.0	125.0
Mixing temperature	153	156.1	157.6	159.2	156.1
Compaction temperature	136.4	140.5	141.2	142.7	139.8

When Table 5 is examined, it is seen that the penetration and ductility values of the modified asphalts decreased up to 5%NS and then increased with the addition of NS. On the other hand, with the increase in the additive ratio, it is observed that the softening point values of the binders increase regularly up to this ratio and then decrease. In this case, it is possible to state that with the addition of NS, the hardening tendency of the binder increases up to 5%NS and the temperature sensitivity decreases. When the viscosity values of the binders are examined in the same table, it is seen that the viscosity values of the modified binders with the addition of NS also increased (especially at the rate of 5%NS) compared to the pure binder. The mixing temperatures in the plant and the compaction temperatures on the road, determined by using these obtained viscosity values, also increased with the increase in the NS additive ratio. All these results show that NS additive hardens the consistency of asphalt binders and therefore more energy can be spent during mixing in the plant and paving-compaction on the road.

### 2.2.2. Preparation of NS added hot mix asphalts

In order to determine the sensitivity of HMAs to water, mixture specimens were prepared by Marshall design method according to ASTM D1559 standard, using pure and NS added asphalts (Figure 2). For this, firstly, optimum asphalt content (OAC) for hot mixes was determined by using aggregate and pure asphalt. Then, based on this content, hot mix specimens were prepared using pure and modified asphalts. For each mixture specimen, 1100 g aggregate was weighed and asphalts were processed at their mixing and compaction temperatures to obtain HMA specimens. The specimens were

prepared by making 75 blows on each surface of the specimen, a total of 150 blows, with the free-dropping hammer from a height of 457 mm.

In the study, pure and NS added mixture specimens were coded as P, P+1NS, P+3NS, P+5NS and P+7NS, respectively.

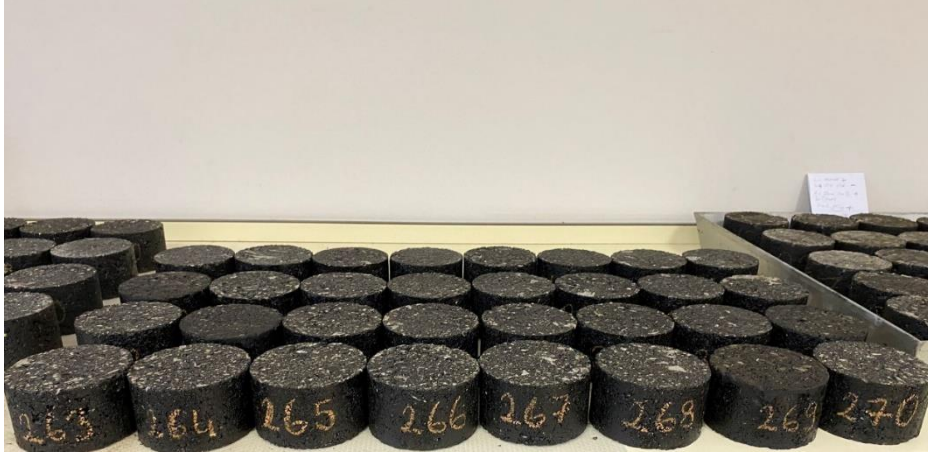


Figure 2. Prepared Marshall briquettes

### 3. Experimental design

#### 3.1. Marshall stability test

The resistance of hot mixtures to plastic flow is determined by Marshall stability and flow test (ASTM D1559). In the experiment, after the heights and weights (in air, water and saturated) of the hot mix specimens are determined, the specimens are kept in a water bath with a temperature of  $60 \pm 1$  °C for approximately 40 minutes. At the end of the time, the specimens are removed from the water bath and placed in the Marshall stability device, and the stability and flow values of the specimens at the time they break at a loading speed of  $50 \pm 2$  mm/min are determined. The stability value indicates the highest load that HMA pavements can resist against deformations, and the flow value indicates the deformation that occurs when this load value is reached. In the experiment, if the heights (h) of the specimens are different from 63.5 mm, the correction coefficients (c) are determined by using the equation (1) [2].

$$c = 5.24e^{(-0.0258h)} \quad (1)$$

Marshall ratio (MQ) values, which are known as a measure of the hardness of hot mixtures and their resistance to deformations, can also be calculated with the help of the stability and flow values obtained as a result of the experiment. The MQ value is obtained by dividing the stability value of the mixture with the flow value, and a high MQ value indicates that the pavement is resistant to deformations [2].

#### 3.2. Retained Marshall stability (RMS) test

The resistance of asphalt pavements to water-induced deterioration can be determined by the RMS test. For this purpose, the mixture specimens are kept in a water bath at  $60 \pm 1$  °C for 24 hours and subjected to loading with Marshall stability device. RMS value is determined by proportioning the obtained stability value to the normal stability value of the specimen. The high RMS value of the mixture specimen indicates that the HMA pavement has higher resistance to water [4].

#### 3.3. Indirect tensile strength (ITS) test

The ITS test is performed to characterize the tensile stresses that occur in the structure of HMA pavements exposed to heat and loads. The test is carried out according to the AASHTO T245 standard and using the Marshall stability

tester. In the test, the mixture specimens are subjected to vertical loading in the direction of the diameter plane at a loading speed of 50 mm per minute, and fracture is ensured. As a result of the experiment, a relationship can be established between these fractures in HMA pavements and the structure of the pavement. With the experiment, information can be obtained about the hardness and durability of the pavement, which are the main parameters of permanent deformation resistance at medium temperatures, and also about the cohesion strength of the HMA pavement. The ITS values of the mixture specimens may vary depending on the cohesion ability of the hot mixture, and this change is largely due to the properties of the asphalt. The ITS value of the mixture specimens can be determined with the help of equation (2). The Pmax value in the equation represents the maximum load applied to the specimen, t the specimen thickness, and d the specimen diameter [2,4].

$$ITS = \frac{2P_{max}}{\pi t d} \tag{2}$$

### 3.4. Water damage resistance test

The sensitivity of HMA pavements to water is commonly determined according to the AASHTO T283 standard. According to the standard, HMA specimens are divided into two groups as “un-conditioned” and “conditioned”. Un-conditioned specimens (ITSdry) are kept in a water bath at 25°C for 2 hours. Conditioned specimens (ITSwet) are first subjected to vacuum treatment so that the air spaces are filled with an average of 70% water. Then, the specimens are wrapped with cling film and frozen in the freezer at -18°C for 16 hours, and at the end of the time, the specimens are kept in a water bath at 60°C for 24 hours. At the end of 24 hours, the specimens taken from the water bath are subjected to the ITS test using the Marshall device after they are kept in the water bath at 25°C for 2 hours. At the end of the experiment, the indirect tensile strength ratio (ITSR) values of the specimens are calculated with the help of equation (3). ITSR values of HMA pavements are expected to be more than 80% in terms of their resistance to water-induced deterioration [2,4].

$$ITSR = (ITS_{wet} / ITS_{dry}) \times 100 \tag{3}$$

## 4. Experimental Results

### 4.1. Marshall stability test results

Hot mix specimens were prepared by using pure B160/220 binder and 1100 g aggregate for the mix design. For this purpose, by keeping the aggregate amount constant, asphalt was added at the rates of 3.5% - 4% - 4.5% - 5% - 5.5% - 6% and 6.5% by weight of the aggregate, and three mixture specimens were prepared for each percentage. After determining the height and various weights (air, water, saturated) of each specimen, the volume specific gravity (Dp), void ratios (Vh), void ratios between aggregates (VMA), and asphalt-filled void ratios (Vf) of all specimens were determined. Then, Marshall stability and flow values of all specimens were determined by Marshall stability device.

The determined volumetric and mechanical properties of the mixture specimens prepared with pure binder are given in Table 6, and the graphs of the change of these properties with asphalt are given in Figure 3.

**Table 6.** Volumetric and mechanical properties of mixture specimens

Asphalt (%)	Dp (g/cm <sup>3</sup> )	Vh (%)	VMA (%)	Vf (%)	Stability (kg)	Flow (mm)
3.5	2.331	8.8	15.03	40.92	1006	2.33
4	2.350	7.4	14.75	49.26	1076	2.58
4.5	2.375	5.8	14.28	58.91	1201	3.07
5	2.399	4.2	13.80	69.30	1236	3.37
5.5	2.411	3.1	13.81	77.28	1199	3.73
6	2.414	2.3	14.08	83.39	1151	3.97
6.5	2.408	1.9	14.70	86.74	1235	3.32

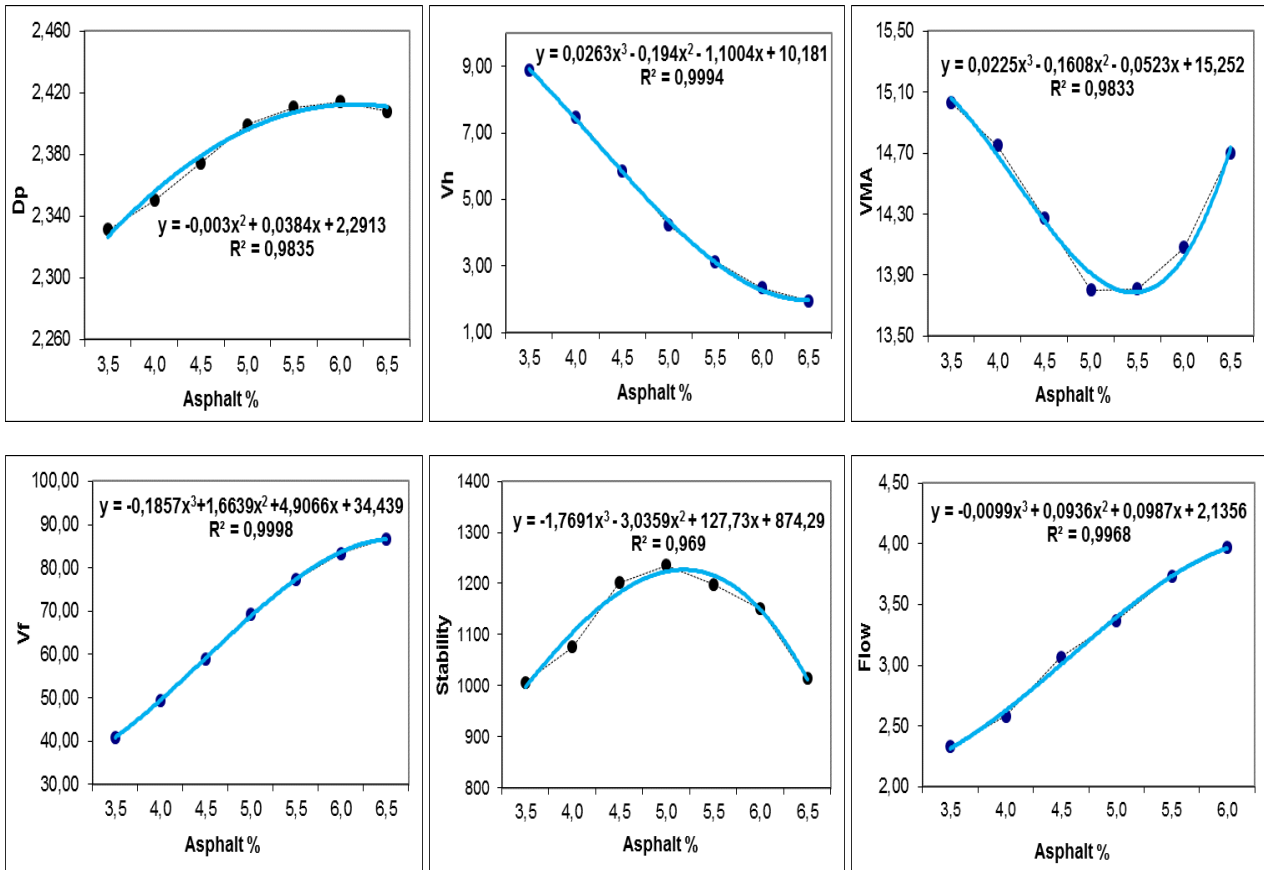


Figure 3. Variation graphs of specimen properties depending on asphalt amount

With the help of the graphics in Figure 3, the optimum asphalt ratio was determined as 5.2% by taking the arithmetic average of four different asphalt percentages, where Dp and stability were maximum, Vh was 4% and Vf was 70%. At this determined ratio, three control specimens were prepared and the compatibility of the results obtained from them was compared with the Highways Technical Specification (HTS) values (Table 7). In the study, it was seen that the results of the control specimens provided the limit values for the surface course of the asphalt concrete in HTS.

Table 7. Results of control specimens

Mixed types	Dp, (g/cm <sup>3</sup> )	Vh, (%)	VMA, (%)	Vf, (%)	Stability, (kg)	Flow, (mm)
P	2.408	4.06	14.71	72.37	1180	2.48
P+1NS	2.410	4.14	14.76	72.32	1226	2.35
P+3NS	2.414	4.17	14.82	73.00	1269	2.24
P+5NS	2.420	4.29	14.96	72.56	1284	2.16
P+7NS	2.421	4.42	14.74	72.48	1204	2.42
HTS	-	3-5	14-16	65-75	>900	2-4

In the study, hot mix specimens were prepared with pure (P) and NS modified binders based on the determined optimum ratio (5.2%). This optimum ratio was kept constant in order to compare the NS added modified mixture specimens with the pure mixture (P) specimens. Marshall stability and flow values obtained from pure and NS added hot mix specimens are shown in Figure 4.

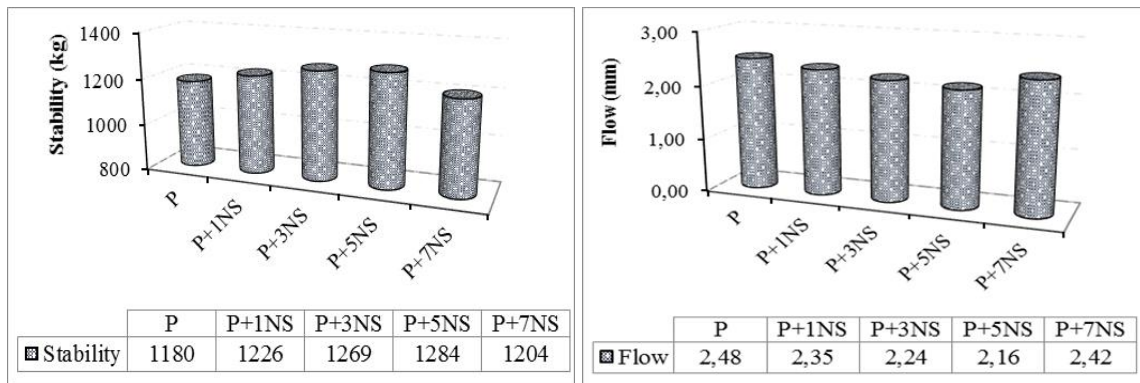


**Figure 4.** Marshall stability and flow values of the mixture specimens

Considering Figure 4, it is seen that the stability values of the mixtures with NS additive increased by 3.9%, 7.5%, 8.8% and 2.0%, respectively, compared to the pure specimen. This increase in the stability values of the mixtures with NS additive shows that NS increases the resistance of asphalt pavements against permanent deformations. When the results are examined, it is seen that the highest stability value is reached in the mixture with 5% NS. In this case, it is possible to state that the mixture with the highest resistance to permanent deformations is the mixture with 5% NS additive. Again, when Figure 4 is examined, the flow values of the mixture specimens with NS additives showed little change compared to the pure (P) mixture specimen. The flow value simulates the plastic or flexible behavior of the pavement under traffic loads. The fact that the flow changes of the specimens remained almost at the same level indicates that there will be no major change in the behavior of the HMA pavement during fracture with the addition of NS.

In the study, MQ values of the specimens were also calculated to determine the hardness and resistance to deformations of all the mixture specimens, and the results are shown in Figure 5.

When Figure 5 is examined, the MQ values of the modified mixtures changed with the increase in the NS ratio. These changes are 9.7%, 19.1%, 24.8% and 4.6% increase compared to the pure (P) mixture. According to these results, it can be stated that the highest increase is seen in the mixture specimens with 5% NS additive, and therefore, the specimens with 5% NS additive are the most resistant to shear stresses.

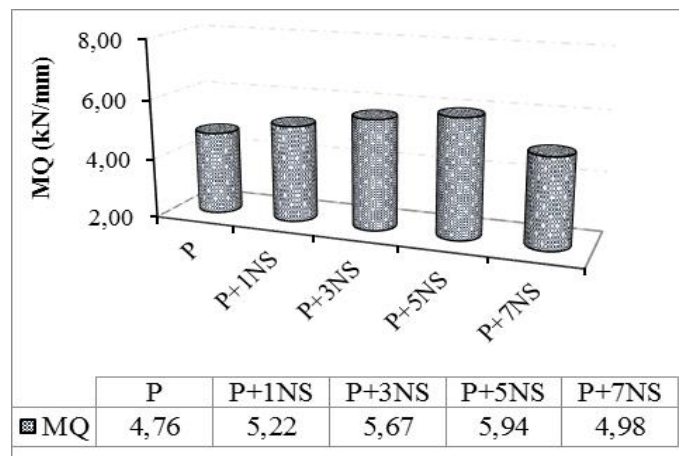


**Figure 5.** MQ values of the mixture specimens

#### 4.2. RMS test results

In order to determine the effects of NS additive on moisture damage resistance of HMA pavements, RMS values of pure and NS added mixture specimens were determined and the results are shown in Figure 6.



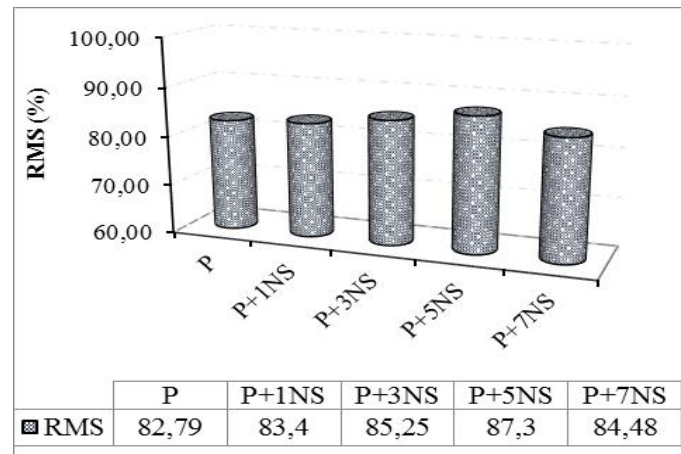


Figure 6. RMS values of mixture specimens

When Figure 6 is examined, it is seen that the RMS values of the modified mixtures change with the increase in NS compared to the pure mixture. These changes occurred as 1.0%, 3.0%, 5.4% and 2.0% increases, respectively, compared to the pure mixture. According to these results, it can be said that the highest RMS value is obtained in mixtures with 5% NS additive, and therefore the highest moisture damage resistance occurs in mixtures with 5% NS additives. As a result, it can be stated that the increase in RMS values with the addition of NS increases the adhesion ability of the NS additive between aggregate and asphalt and has an improving effect on the cohesion ability of the mixture, and therefore NS causes an increase in the moisture resistance of the pavement.

### 4.3. ITS and moisture resistance test results

In order to determine the effects of NS on the moisture resistance of HMA, the prepared conditioned and unconditioned pure (P) and NS added mixture specimens were subjected to the ITS test. The determined ITS and ITSR values of the specimens are given in Figure 7 and Figure 8, respectively.

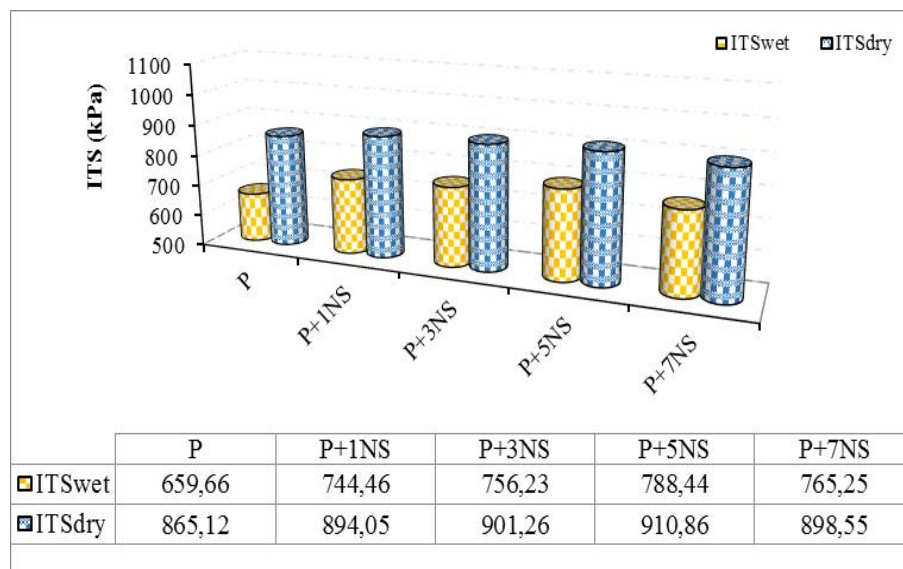


Figure 7. ITS values of mixture specimens

When Figure 7 is examined, the tensile strength values of the conditioned mixture specimens (ITSwet) with the increase of NS increased by 12.9%, 14.6%, 19.5% and 16.0%, respectively, compared to the pure mixture (P). On



the other hand, ITS values of unconditioned mixture specimens (ITS<sub>dry</sub>) increased by 3.3%, 4.2%, 5.3% and 3.9%, respectively. The increase in the ITS<sub>wet</sub> and ITS<sub>dry</sub> values of the specimens with the increase in the NS additive ratio in the mixture shows that the resistance of the HMA pavement, which is exposed to traffic loads, against the tensile stresses that can occur under these loads increases.

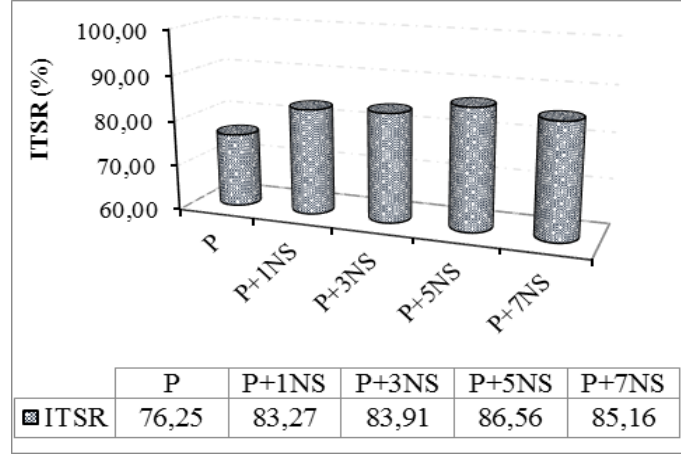


Figure 8. ITSR values of mixture specimens

When Figure 8 is examined, with the increase of the NS additive ratio, the ITSR values of the mixture specimens increased by 9.2%, 10.0%, 13.5% and 11.7%, respectively, compared to the pure mixture. According to these results, the highest ITSR value was observed in the mixture with 5% NS. The fact that the ITSR values of the NS added specimens were higher than 80% indicates that the NS additive improves the cohesion ability of the mixtures and makes the pavements more durable in terms of moisture resistance. For this reason, it is possible to state that modified hot mixtures prepared by adding NS will have high resistance to deterioration caused by water effects.

When the RMS and ITSR results are evaluated together, it has been determined that the NS additive has a positive effect on the moisture resistance of the road pavements by increasing the adhesion and cohesion ability of the mixtures, especially by 5% NS.

## 5. Conclusions

In the study, the effects of nanosilica (NS) additive on the resistance of road pavements to the harmful effects of water were investigated and the following results were obtained.

- ✓ When the physical results of the pure and NS added binders were evaluated, it was observed that the consistency of the asphalts with NS additive was hardened and the binder class changed to B 100/150.
- ✓ According to Marshall stability results, it was observed that the stability of the mixtures increased by 8.8% with NS additive and the highest stability value was obtained from the mixtures with 5% NS additive.
- ✓ According to the MQ results, the highest MQ value was obtained from the mixtures with 5% NS additive and it was observed that the NS additive provided an improvement in the resistance of HMA pavements to shear stresses.
- ✓ According to the RMS results, it was observed that there was an increase of 5.4% in the resistance of the hot mixtures against the effects of moisture with the addition of NS, and this increase was obtained from the mixtures with 5% NS.

- ✓ According to the ITSR results, it was observed that the highest value was obtained from the mixtures with 5% NS addition and the addition of NS improved the moisture resistance of the road pavements by 13.5% by increasing the adhesion and cohesion ability of the hot mixtures.
- ✓ It is considered that it may be useful to investigate the effect of nanosilica additive on the moisture resistance of the mixture by adding it directly to the hot mixture in future studies.

As a result, it is possible to state that the use of nanosilica (NS) additive in modification has an improving effect on the sensitivity of road pavements to water by increasing the stability, shear and moisture resistance of hot mixes.

## 6. Author Contribution Statement

In the study, Author 1 and Author 3 contributed to forming the idea, the analysis of the results, provision of the materials and examination of the results; Author 2 contributed making the design, the analysis of the results, checking the article in terms of content and literature review.

## 7. Ethics Committee Approval and Statement of Conflict of Interest

There is no need for an ethics committee approval in the prepared article. There is no conflict of interest with any person/institution in the prepared article.

## 8. References

- [1] El-Maaty Behiry AEA. "Laboratory evaluation of resistance to moisture damage in asphalt mixtures". *Ain Shams Engineering Journal*, 4(3), 351-363, 2013.
- [2] Geçkil T, Aksağan Z, İnce CB. "Asfalt kaplamaların nem performansı üzerinde siyah karbonun etkisi". *Düzce Üniversitesi Bilim ve Teknoloji Dergisi*, 9(5), 2101-2115, 2021.
- [3] Omar HA, Yusoff NIM, Mubarakı M, Ceylan H. "Effects of moisture damage on asphalt mixtures". *Journal of Traffic and Transportation Engineering (English Edition)*, 7(5), 600-628, 2020.
- [4] Geçkil T, Seloğlu M, İnce CB. "Sıcak karışım asfalt kaplamanın su hasarı direnci üzerinde RET katkısının etkisi". *Firat Üniversitesi Mühendislik Bilimleri Dergisi*, 33(2), 537-546, 2021.
- [5] Görkem Ç, Şengöz B. "Predicting stripping and moisture induced damage of asphalt concrete prepared with polymer modified bitumen and hydrated lime". *Construction and Building Materials*, 23 (6), 2227-2236, 2009.
- [6] Özen H. "Rutting evaluation of hydrated lime and SBS modified asphalt mixtures for laboratory and field compacted samples". *Construction and Building Materials*, 25 (2), 756-765, 2011
- [7] Petersen JC, Plancher HP, Harnsbergen M. "Lime treatment of asphalt to reduce age hardening and improve flow properties". *In: Proceedings AAPT*, 56, 632-653, 1987.
- [8] Kennedy TW, Anagnos NJ. "Lime treatment of asphalt mixtures", 4. *Center for Transportation Research*, Austin, United States, 20-28, 1983.
- [9] Epps J, Berger E, Anagnos JN, "Moisture sensitivity of asphalt pavements." *A National Seminar*, California, United States, 117-177, 2003.
- [10] Kumar P, Chandra S, Bose S. "Strength characteristics of polymer modified mixes". *International Journal of Pavement Engineering*, 7(1), 63-71, 2006.
- [11] Lazzara G, Milioto S. "Dispersions of nanosilica in biocompatible copolymers". *Polymer Degradation and Stability*, 95 (4), 610-617, 2010.
- [12] Geçkil T, İnce CB, Özpınar ET. "Nanosilikanın bitümün kıvamı, viskozitesi ve mikroyapısına etkileri". *Konya Mühendislik Bilimleri Dergisi*, 9(4), 845-857, 2021.
- [13] Shafabakhsh G, Akbari M, Bahrami H. "Evaluating the fatigue resistance of the innovative modified-reinforced composite asphalt mixture". *Advances in Civil Engineering*, 1-10, 2020.
- [14] Shafabakhsh G, Motamedi M, Firouznia M, Isazadeh M. "Experimental investigation of the effect of asphalt binder modified with nanosilica on the rutting, fatigue and performance grade". *Petroleum Science and Technology*, 37(13), 1495-1500, 2019.

- [15] Chen X, Liu S, Sun L. “Preparation and properties of emulsion asphalt modified by nanosilica/SBR composite”. *China Rubber Industry*, 54, 337-340, 2007.
- [16] Nazari H, Naderi K, Moghadas Nejad F. “Improving aging resistance and fatigue performance of asphalt binders using inorganic nanoparticles”. *Construction and Building Materials*, 170, 591–602, 2018.
- [17] Shafabakhsh G, Sadeghnejad M, Ebrahimnia R. “Fracture resistance of asphalt mixtures under mixed-mode I/II loading at low-temperature: without and with nano SiO<sub>2</sub>”. *Construction and Building Materials*, 266, 2021.
- [18] Yao H. “Rheological properties and chemical bonding of asphalt modified with nanosilica”. *Journal of Materials in Civil Engineering*, 25(11), 1619-1630, 2013.
- [19] Sun L, Xin X, Ren J. “Asphalt modification using nano-materials and polymers composite considering high and low temperature performance”. *Construction and Building Materials*, 133, 358-366, 2017
- [20] Yusoff NIM. “Evaluation of fatigue behavior of asphalt layers containing nanosilica modified tack coat”. *Advances in Materials Science and Engineering*, 1-11. 2022.



## Classification of recyclable waste using deep learning architectures

### Derin öğrenme mimarileri kullanılarak geri dönüştürülebilir atıkların sınıflandırılması

Arzu SEVİNÇ<sup>1\*</sup> , Fatih ÖZYURT<sup>2</sup> 

<sup>1,2</sup>Department of Software Engineering, Faculty of Engineering, Firat University, Elazig, Turkey.

<sup>1</sup>arzusevinc99@gmail.com, <sup>2</sup>fatihozyurt@firat.edu.tr

Received: 14.09.2022  
Accepted: 07.10.2022

Revision: 21.09. 2022

doi: 10.5505/fujece.2022.83997  
Research Article

#### Abstract

Managing waste in big cities is a big problem. Wastes are dangerous in terms of causing environmental pollution and affecting human health. In particular, solid wastes such as glass and plastic do not dissolve in the soil for a long time and pollute the environment. By recycling such solid wastes, the surrounding waste can be reduced. Therefore, it is important to classify waste and to recycle the separated waste. In this study, a data set consisting of 22500 waste images was used. The data set contains color image data with a size of 227 x 227 pixels. The data used in the study are divided into two as organic and recyclable waste. This study proposes a deep learning-based system for classifying waste. With such a system, wastes can be classified and recycled. The data was trained with the ResNet 50 architecture and the CNN architecture created to classify waste, and accuracy rates were compared. The CNN architecture created to classify waste is more successful for this data set with an accuracy rate of 91.84%.

**Keywords:** Waste classification, Deep learning, Convolutional neural network, ResNet-50 architecture.

#### Özet

Büyük şehirlerde atıkların yönetilmesi büyük bir problemdir. Atıklar çevre kirliliğine sebep olması ve insan sağlığını etkilemesi açısından tehlikelidir. Özellikle cam, plastic gibi katı atıklar toprakta uzun süre çözünmeyerek çevreyi kirletmektedir. Bu tarz katı atıklar geri dönüştürülerek çevredeki atıklar azaltılabilir. Bu yüzden atıkları sınıflandırmak ve ayrıştırılan atıkların geri dönüştürülmesi önemlidir. Bu çalışmada 22500 atık görüntüden oluşan bir veri seti kullanılmıştır. Veri seti, 227 x 227 piksel boyutundaki renkli görüntü verilerini içermektedir. Çalışmada kullanılan veriler, organik ve geri dönüştürülebilir atık olarak ikiye ayrılmaktadır. Bu çalışma atıkları sınıflandırmak için derin öğrenme tabanlı bir sistem önermektedir. Bu tarz bir sistemle atıklar sınıflandırılarak geri dönüştürülebilir. Veriler ResNet 50 mimarisi ve atık sınıflandırmak için oluşturulan CNN mimarisi ile eğitilerek doğruluk oranları karşılaştırıldı. Atık sınıflandırmak için oluşturulan CNN mimarisi %91,84 doğruluk oranı ile bu veri seti için daha başarılı olduğu görülmektedir.

**Anahtar Kelimeler:** Atıkların sınıflandırılması, Derin öğrenme, Evrişimsel sinir ağı, ResNet-50 mimarisi.

## 1. Introduction

There is an increasing waste management problem around the world. Tons of waste are discarded every year, and this number increases every year. With the development of industry in major cities, waste management has become even more difficult. the waste count is estimated to be 2.2 billion tons by 2025 [1]. As waste increases, it is more difficult to create free space for waste with the effect of urbanization. In this case, it is often seen that the waste is burned. However, the burning of waste causes air pollution, which triggers cancer. So waste is a danger to the environment and human health.

Recycling waste is an environmentally and economically useful method. In this way, raw resources can be recovered, energy can be preserved, air and water pollution can be reduced, and parts allocated for the refuse area can be reduced. Countries have started implementing some systems to recycle waste. Important steps are taken for the waste problem, especially in a crowded country like China. There has been a recent study of artificial intelligence integrated in order to classify waste.

\*Corresponding author

Many countries have done research in this area to recycle waste. Scientists have shown that waste can be classified with an autonomous system using image classification techniques. A study in this area uses thermal imaging techniques to classify recyclable materials. This technique has achieved success from 85% to 96% [2].

The classification and recycling of waste is essential for a healthy life. However, different types of waste make this classification difficult. Through deep learning methods, images are reviewed for the classification of waste, so recyclable waste can be classified. The excess of waste types and the difficulty of their solution are the main reason scientists are concentrating on deep learning methods for waste management. In an investigation, the image is classified with AlexNet, DenseNet169, VGG16, GoogleNet models, and then DenseNet169 image classification models based on transfer learning are used. Compared to these methods, the DenseNet169 models based on transfer learning were found to have an 82.8% accuracy and a higher success than other models [3]. In another study in this area, the TrashNet dataset was trained using the DenseNet121 architecture. DenseNet121 architecture achieved a high accuracy rate of 99.6% with this data set [4]. Another study conducted a system using the R-CNN model to determine the size when using CNN to classify. This system has been successful with accuracy rates from 90% to 96.7% [5]. In this research, paper, glass, plastic and organic wastes were classified using DCNN architectures. The highest success has been achieved in the classification of organic wastes. In organic waste, the 5-layer DCNN architecture achieved a 76.7% accuracy rate and the 4-layer DCNN architecture achieved an 83% accuracy rate [6]. A study using the TrashNet dataset uses a ResNet18-based image classification model to classify waste. This successful model has an accuracy of 95.87% [7]. In a system created using deep learning-based classifier and cloud computing technique, waste is divided into 6 categories. In this study, the classifier created using Mobilenetv3 architecture achieved a good result with a accuracy rate of 94.24% [8]. The deep learning method has shown successful results in the classification of waste.

**Table 1.** Comparison of publications in the literature

Method	Accuracy
Thermal Imaging Techniques [2]	%85 - %96
DenseNet169 [3]	%82,8
DenseNet121 [4]	%99,6
R-CNN [5]	%90 - %96,7
Four layer DCNN and five layer DCNN [6]	%83 and %76,7
ResNet-18 [7]	%95,87
MobileNetV3 [8]	%94,12

This study is a study to recycle waste. In the study, it was aimed to classify the wastes by using a data set consisting of two categories. The wastes in the data set are divided into organic and recyclable. The data is trained using two different architectures. First, the data set was trained using the CNN architecture created for the classification of waste. The dataset was then trained using the Resnet50 architecture. Finally, the success rates obtained from the training of the two architects were compared and it was determined which architecture would be more successful for this study.

## 2. Method and Material

### 2.1. Dataset

The dataset used in this study was accessed via Kaggle [9]. The images in the dataset are divided into organic and recyclable. Contains 22500 data consisting of color images. This image data has 227 x 227 pixels. Figure 1 shows the organic waste images in the dataset and Figure 2 shows the recyclable waste images. Organic waste is usually made up of foods such as vegetables and fruits that can be thawed out in nature. The recyclable waste consists of waste such as glass, plastic, nylon, wood, metal.

The problem of classification of wastes is important for the environment and human health all over the world. This data set was used to solve the problem of waste classification. The data set used is divided into two categories as recyclable and organic waste. Organic wastes that can be dissolved in the soil are wastes that are not harmful to the environment. Wastes such as glass, plastic which does not dissolve in the soil for years, are recyclable wastes. Classification of wastes and determination of recyclable wastes will solve our problem. In this respect, the data set used in the study is sufficient for the solution of the problem of classification of wastes.



Figure 1. Organic waste images in dataset

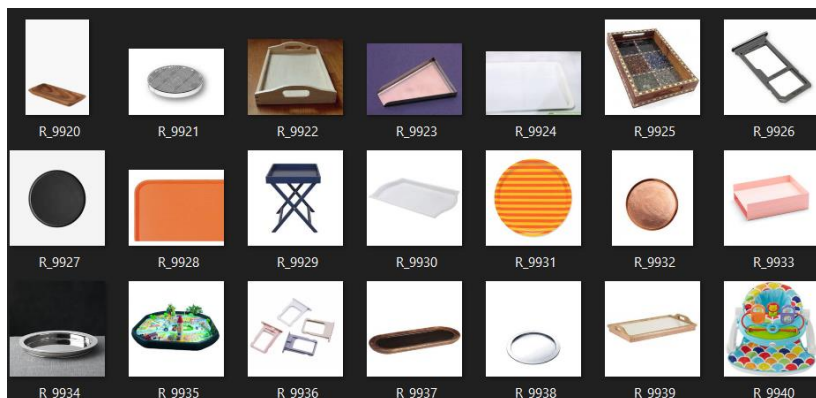


Figure 2. Recyclable waste images in dataset

## 2.2. Waste classification model based on CNN Architecture

CNN is an algorithm that can extract properties of objects in an image and distinguish objects from each other. The convolutional neural network is a mathematical structure composed of multiple layers and uses the process of convolution. Convolution is a mathematical process that produces a new function that shows how a shape is changed by another shape. CNN consists of a layer of input, an output layer, and different layers between these two layers. The middle layers are the layers that perform mathematical operations (convolution).

The convolution layer is the layer that extracts the properties of the image. A filter matrix is created in the convolution layer and circulated over the image. The pooling layer is used to reduce data size and processing time. Important information is preserved while reducing size. There are different types of pooling. The first is the maximum pooling, which uses the maximum value of the neuron clusters. The average pooling extracts an average value from these clusters and uses that value. The collection of all neuron values is total pooling. The fully connected layer has been named because the neurons on the layers are completely connected to each other. The matrices pass through fully connected layers to sort the image.



A CNN model has been created for this study. This CNN model is shown in Figure 3. The model consists of 5 convolution layers, 5 pool layers, and 3 fully connected layers. The activation function uses the sigmoid function. The curve of this nonlinear function is similar to the S shape. The values obtained from the Sigmoid function are between 0 and 1. When calculating the probability of anything, the sigmoid function is usually preferred.

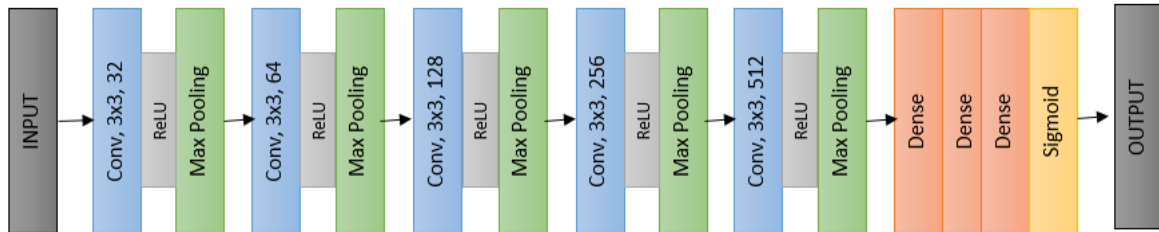


**Figure 3.** The basic structure of CNN architecture for the classification of waste

CNN architecture includes 5 convolution layers, 5 pooling layers and 3 full link layers. There is a ReLU activation function between the convolution layer and the pooling layer. After the full link layer, there is a Sigmoid activation function. The block diagram for this architecture is shown in Figure 4.

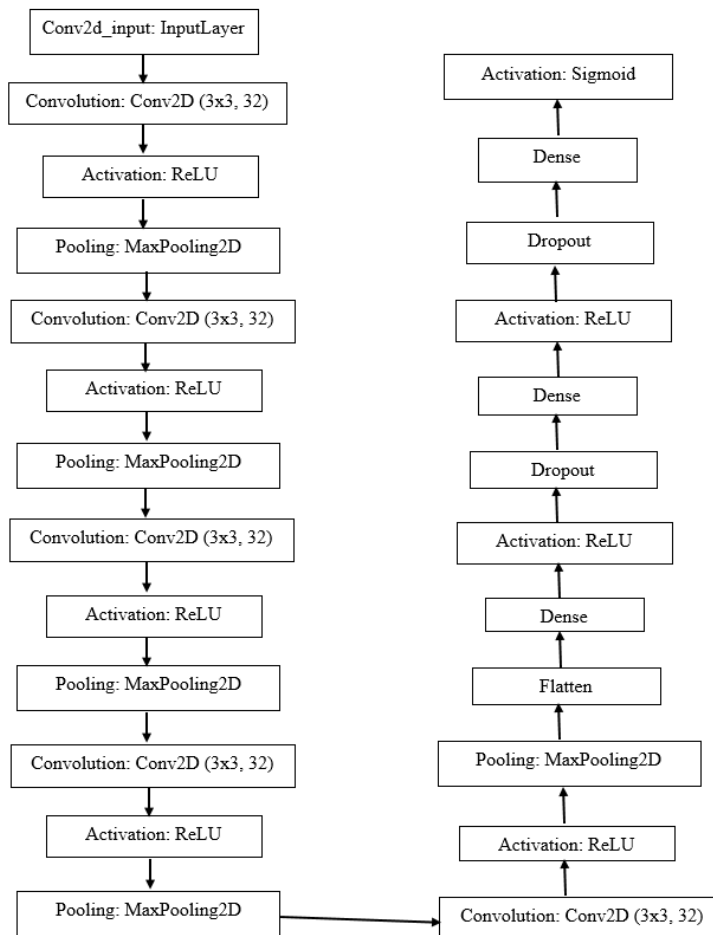


**Figure 4.** Block diagram of CNN architecture



### 2.3. ResNet 50 Architecture

ResNet [10], has won the ILSVRC-2015 competition. It consists of up to 152 layers of convolution. The ResNet 50 architecture has a 50-layer depth. The ResNet architecture uses short paths. These short paths contribute to reduced deterioration and increased operating speed. Figure 4 contains an image of the ResNet 50 architecture.

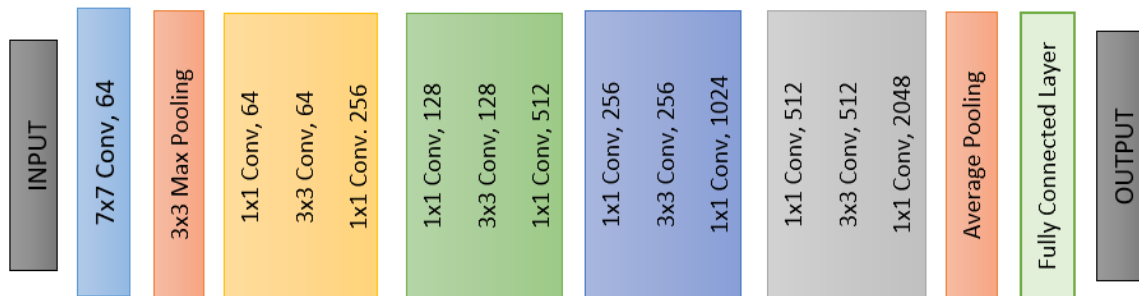


Figure 5. The basic structure of Resnet 50 architecture, a pre-trained CNN architecture

### 3. Result and Discussion

Convolutional neural network models are used to classify waste. Data is trained using the Resnet 50 architecture, and the CNN architecture created for this study. The accuracy rates obtained as a result of the training are compared.

The graphic of data trained with CNN architecture is shown in Figure 5. The figure has accuracy and loss graphics. This architecture has an accuracy of 91.84%. The CNN architecture created uses 5 convolution layers, 5 pool layers, and 3 fully connected layers. It also uses sigmoid as an activation function.

The dataset used contains 22500 waste images. 85% of data is used for training and 15% for testing.

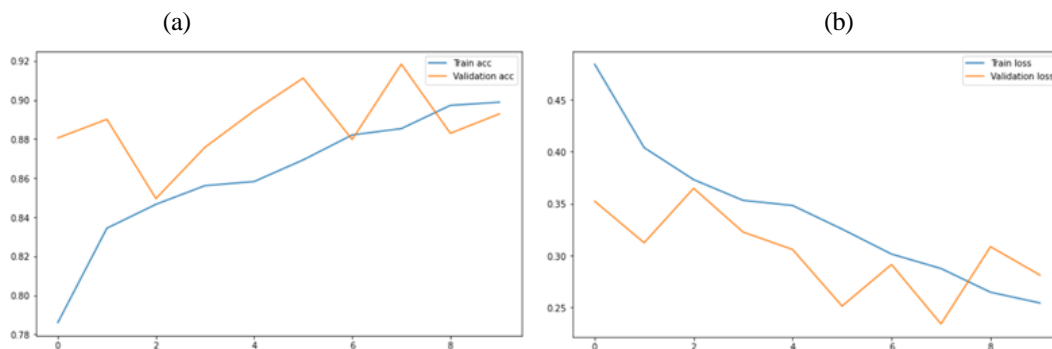
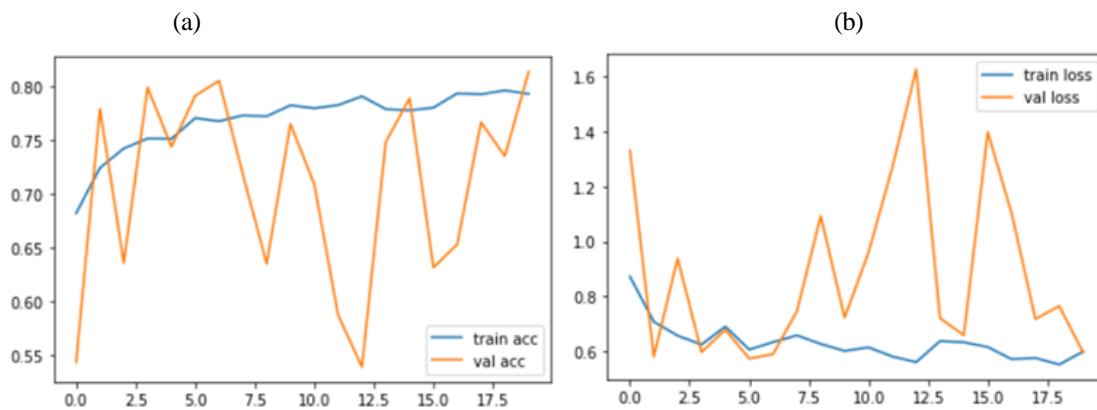


Figure 6. Graphics for CNN architecture. (a) Accuracy plot, (b) Loss plot

The accuracy plot as a result of training the Resnet 50 architecture with this data is shown in figure 1. The highest accuracy obtained was 81.34%. The Resnet architecture is an architecture with a depth of 50 layers. As the activation function, it uses the softmax function. The Softmax function is the activation function that interprets the numbers according to the possibilities [11].

85% of the data used here is used for training and 15% for testing. Waste data is color and 227x227 pixel size data.



**Figure 7.** Graphics for Resnet-50 architecture. (a) Accuracy plot, (b) Loss plot

Results graphics from the training of both architects were given above. When the results are analyzed, it is seen that the CNN architecture were created to classify waste is better. CNN architecture has a 91.84% accuracy ratio, while ResNet50 architecture has an 81.34% accuracy ratio. There is a 10.54% difference between them. For deep learning, this difference is a high difference.

#### 4. Conclusions

The purpose of this study is to ensure that highly produced waste is classified so that it can be recycled. The data used in this study is divided into organic and recyclable. The dataset contains a total of 22500 waste image data. This data has been trained using Resnet50 and Cnn architecture. By studying the accuracy rates obtained as a result of the inclination, it was determined which architecture was more successful. The training of CNN architecture resulted in a 91.84% accuracy ratio. The ResNet50 architecture achieved an 81.34% accuracy ratio. CNN architecture is seen to be more successful in the classification of waste for this dataset.

#### 5. Author Contribution Statement

In this study, Author 1 contributed making the design, literature review, contributed to forming the idea, the analysis of the results; Author 2 contributed to checking the spelling and checking in terms of content.

#### 6. Ethics Committee Approval and Statement of Conflict of Interest

“There is no need for an ethics committee approval in the prepared article”

“There is no conflict of interest with any person/institution in the prepared article”

#### 7. References

- [1] Hoornweg D, Bhada-Tata P. "What a waste: a global review of solid waste management". <https://openknowledge.worldbank.org/handle/10986/17388> (12.09.2022).
- [2] Gundupalli S.P, Hait S, Thakur,A. "Multi-material classification of dry recyclables from municipal solid waste based on thermal imaging". *Waste Management* , 70, 13-21, 2017.
- [3] Zhang Q, Yang Q, Zhang X, Bao Q, Su J, Liu X. "Waste image classification based on transfer learning and convolutional neural network". *Waste Management*, 135, 150-157, 2021.
- [4] Mao WL, Chen LW, Wang CT, Lin YH. "Recycling waste classification using optimized convolutional neural network". *Resources, Conservation and Recycling*, 164, 105132, 2021.
- [5] Nowakowski P, Pamuła T."Application of deep learning object classifier to improve e-waste collection planning". *Waste Management*, 109, 1-9, 2020.

- [6] Altikat A, Gulbe A, Altikat S. " Intelligent solid waste classification using deep convolutional neural networks". *International Journal of Environmental Science and Technology*, 19(3), 1285-1292, 2022.
- [7] Zhang Q, Zhang X, Mu X, Wang Z, Tian R, Wang X, Liu X. "Recyclable waste image recognition based on deep learning". *Resources, Conservation and Recycling*, 171, 105636, 2021.
- [8] Wang C, Qin J, Qu C, Ran X, Liu C, Chen B. "A smart municipal waste management system based on deep-learning and Internet of Things". *Waste Management*, 135, 20-29, 2021.
- [9] Sekar S. "Waste Classification data". <https://www.kaggle.com/datasets/techsash/waste-classification-data> (08 09 2022).
- [10] He K, Zhang X, Ren S, Sun J. "Deep residual learning for image recognition". In *Proceedings of the IEEE Conference On Computer Vision and Pattern Recognition, Las Vegas, NV, USA, 27-30 June 2016*.
- [11] Sharma S, Sharma S, Athaiya A. "Activation functions in neural networks". *Towards Data Science towards data science*, 6(12), 310-31, 2017.



## Failure mechanism of a soil slope and stabilization method: a case study

### Bir zemin şevinin yenilme mekanizması ve stabilizasyon yöntemi: vaka çalışması

Mustafa KANIK<sup>1\*</sup>

<sup>1</sup>Department of Geological Engineering, Faculty of Engineering, Firat University, Elazig, Türkiye.  
[mkanik@firat.edu.tr](mailto:mkanik@firat.edu.tr)

Received: 10.10.2022  
Accepted: 25.10.2022

Revision: 22.10.2022

doi: 10.5505/fujece.2022.35744  
Case Report

#### Abstract

In this study, the slope stability problem, which occurred when the projected excavation works of a treatment plant has been started, has been examined. The aim of this study is to determine the conditions causing the slope failure and to make the slope stable again. Then, to ensure the stability of the whole slope after all the excavations work in the project area have been completed. For this purpose, firstly, the topographic features of the slope where the failure took place were determined and a model of the failure condition was created. Field and laboratory studies were used to obtain the data to be used in slope modeling. Models reflecting the current situation were analyzed considering static and dynamic conditions and a safe slope design was created. The analyzes are carried out by Slide V.6.0. software which is based on limit equilibrium methods and Bishop Method was preferred. As a result, it was determined that the reason of the failure occurred was the change of the soil's physical and mechanical parameters due to precipitation. In the slope stability problem considered, the benching method has been proposed as an improvement method, and additionally, suggestions have been made for the disposal of surface waters by drainage methods.

**Keywords:** Limit equilibrium, Slide, Slope stability.

#### Özet

Bu çalışmada bir arıtma tesisinin projelendirilmiş kazı çalışmalarına başlandığında oluşan şev stabilitesi problemi incelenmiştir. Bu çalışmanın amacı, şev duraysızlığına neden olan koşulları belirlemek ve şevi tekrar duraylı hale getirmektir. Daha sonra proje alanındaki tüm kazı çalışmaları tamamlandıktan sonra tüm şevin stabilitesini sağlamaktır. Bu amaçla öncelikle duraysızlığın meydana geldiği şevin topografik özellikleri belirlenmiş ve duraysızlık durumunun bir modeli oluşturulmuştur. Şev modellemeye kullanılacak verilerin elde edilmesi için arazi ve laboratuvar çalışmalarından yararlanılmıştır. Mevcut durumu yansıtan modeller statik ve dinamik koşullar dikkate alınarak analiz edilerek güvenli bir şev tasarımı oluşturulmuştur. Analizler limit denge yöntemlerine dayalı Slide V.6.0 paket programı ile gerçekleştirilmiştir ve Bishop Metodu tercih edilmiştir. Sonuç olarak, meydana gelen duraysızlığın nedeninin yağış nedeniyle zeminin fiziksel ve mekanik parametrelerinin değişmesi olduğu tespit edilmiştir. Ele alınan şev stabilitesi probleminde iyileştirme yöntemi olarak basamaklama yöntemi önerilmiş ve ayrıca yüzey sularının drenaj yöntemleriyle bertarafı için önerilerde bulunulmuştur.

**Anahtar kelimeler:** Limit denge, Slide, Şev stabilitesi.

## 1. Introduction

After floods, storms, and earthquakes landslides take the fourth place in the fatal natural disasters. Beside its comprehensive coverage, high frequency, and incredible destructive power [1] landslides cause significant casualties and property damage every year around the world [2 - 4]. It is possible to define two types of slopes as natural and constructed. The fact that slopes are natural or constructed does not lead slopes to stable conditions. As a result of exceeding the shear strength of the soil, a failure occurs on the slope. The shear stresses that occur along the force action surface causing this failure are determined and compared in terms of the shear strength parameters of the soil. Calculations performed using these parameters are called slope stability analyses [5].

\*Corresponding author

The failure of slopes gives information about the soil and conditions at the time of failure. By performing back analyzes, the strength parameters of the soils in the study areas, the state of the groundwater and the failure model are tried to be understood [6]. As a result of these analyzes, the process of determining the failure status of a slope, the soil conditions at the time of failure and the appropriate sliding model for the situation is called back-analysis [7].

For the analysis performed at the moment of failure, the soil strength parameters and pore water pressure parameters at this moment should be taken as a basis [8]. For back analysis, many researchers used both deterministic methods [9], [10 - 13] as well as probabilistic methods [14 - 16]. Discontinuities, underground and environmental waters, soil parameters, earthquake etc. dynamic effects and slope geometry are the most important parameters controlling the stability of both natural and constructed slopes.

Shallow and deep-seated landslides innately differ in their size, extent and the risk posed [17]. Such landslide types reflect a variety of environmental and geological factors [18]. Separating these two landslide types is helpful for the protection from causalities [19 - 21].

In this study, slope stability analyzes were performed using the limit equilibrium software, Slide v.06 [22]. In this study, the cause of a failure occurred after excavation works started in a water treatment construction project area was tried to be determined for the existing ground conditions. For the slope in the same region where no failure has occurred yet, different analyzes were carried out and the stability of the slope was examined under the dynamic and static conditions. Then, precautions to be taken for possible situations have been determined.

## **2. Material and Method**

In this study, to determine the Factor of Safety value, one of several Methods of Slices is used, The Bishop Method [23]. The assumptions made regarding the interslice forces differs the approach from the Ordinary Method of slices. The Bishop method neglects the shear interslice forces acting at the lateral sides of each slice. Bishop used three main equilibrium equations; moment equilibrium, horizontal force equilibrium and vertical force equilibriums. The factor of safety value for a typical circular failure surface is derived and it is assumed that the failure surface lies within a single type of soil which behaves in accordance with the Mohr-Coulomb failure criterion [24].

In this study, Slide v.6.0 software, using Simplified Bishop Method as an option, was preferred to evaluate the failure mechanism of the slope. The Bishop Method was preferred because it can be applied to soil and rock masses that have gained soil characteristics by weathering. As it was stated by many researchers, in the circular surface assumptions the given factor of safety values by Bishop Method are in good agreement with the factor of safety values of other rigorous methods. This method is basically the same as the Swedish Method, but it takes account the force between the existing slices so the method gives more accurate factor of safety values.

## **3. Slope Stability Analysis**

It is desired to build a water treatment plant in the region where failure occurs. Excavations were started in this area, but after the excavations have started, a failure occurred (Figure 1). Before seeking for the reasons of the failure the data about the soil should be collected. In the study area is formed of Miocene-Pliocene aged Şelmo Formation, first defined by Bolgi [25]. The Şelmo Formation starts with fine grained conglomerate at the bottom. It consists of cross-bedded, dough-supported, magmatic grains, limestone, sandstone, and the matrix consists of sand and clay [26]. The Şelmo Formation bears traces of fluvial deposits in its upper parts. Therefore, if the Şelmo Formation is considered as a whole, it can be named as fan deposits [27, 28].



**Figure 1.** The area where the failure in the study area occurs

Before starting the analysis, the region where the failure started was evaluated within itself, then the regions where any problem did not occur were examined in terms of possible problems and analyzes were carried out for static and dynamic situations on the specified lines. The lines have been chosen considering the regions where the excavations will take place (Figure 2). Topographic sections were determined by the studies carried out by survey engineers. Samples were collected after the failure happened. As a result of the experiments performed on the samples obtained, it was determined that the soil is CH and the unit weight of the soil is  $19 \text{ kN/m}^3$ . The mean internal friction angle is  $14^\circ$  and the mean cohesion value is  $71.48 \text{ kN/m}^2$ . Ground acceleration values used in dynamic analyzes were selected according to the area of the parcel where the project took place, and the PGA (peak ground acceleration) value was specified as  $0.177 \text{ g}$  (Figure 3).

### 3.1. Failure Mechanism

The first model (Line I) was created by considering the excavations to be carried out in accordance with the project within the slope surface with an average inclination of  $8.5^\circ$ . In the prepared cross-sections, the lower elevation of the slope was measured as 672.5 and the upper elevation as 728 m. For the slope to be created during excavation, the sliding mass due to the failure (Figure 2) must be removed. As a result of this, the slope to be formed was considered as a single step and the lower elevation of this slope was given as 679 and the upper elevation as 704.50 by the survey engineers.

As a result of the analysis, the static state safety factor for the natural slope was obtained as 1.299 (Figure 4). This indicates that the factor of safety of the slope is sufficient for the given condition.

Considering the seismicity of the region, the same slope was remodeled under dynamic conditions and analyzes were carried out. The PGA value of the region in which the study area is located was specified as  $0.177 \text{ g}$  (Figure 3). When the results of the analysis are examined, the lowest safety factor for the slope is 0.998 and the structures to be built are within the effect limits of the possible failure shown in Figure 6.



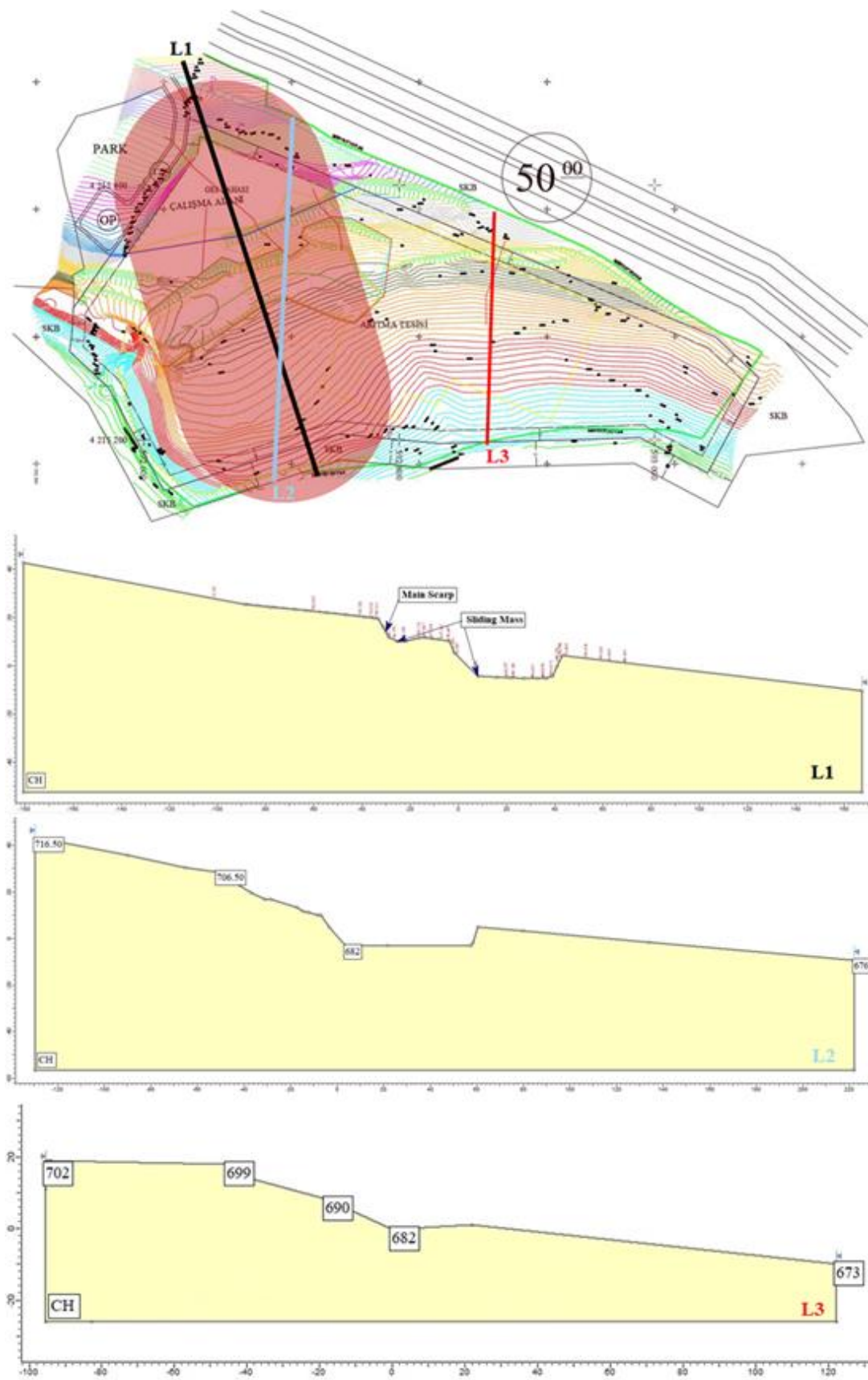


Figure 2. Instable area red circled and studied lines (L1, L2 and L3)



## Turkiye Earthquake Hazard Maps Interactive Web Application

### User Inputs

Report Title	Slope Stability	
Earthquake ground motion level	DD-2	Earthquake ground motion level with 10% probability of occurrence in 50 years (Recurrence period 475 years)
Soil Class	ZC	layers of gravel and hard clay or weathered, highly fractured weak rock
Latitude	38.0652	
Longitude	40.05051	

### Outputs

$S_s = 0.407$	$S_1 = 0.152$	$PGA = 0.177$	$PGV = 12.252$
---------------	---------------	---------------	----------------

$S_s$  : Short period map spectral acceleration coefficient (dimensionless)

$S_1$  : Map spectral acceleration coefficient for 1 second period (dimensionless)

PGA : Peak ground acceleration (g)

PGV : Peak ground velocity (cm/sn)

**Figure 3.** Peak Ground Acceleration (PGA) value

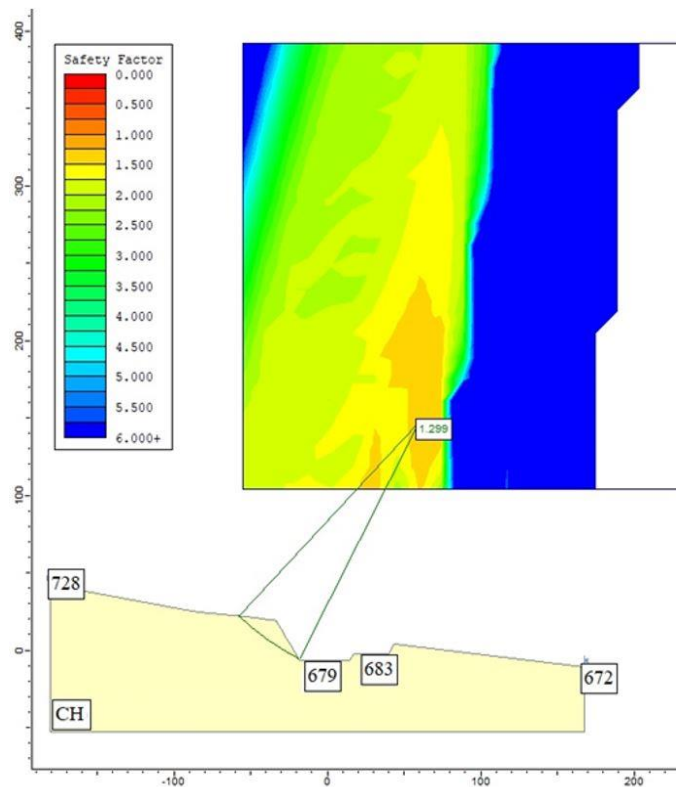


**Figure 4.** The minimum factor of safety (1.29) obtained for the static condition for Line-I

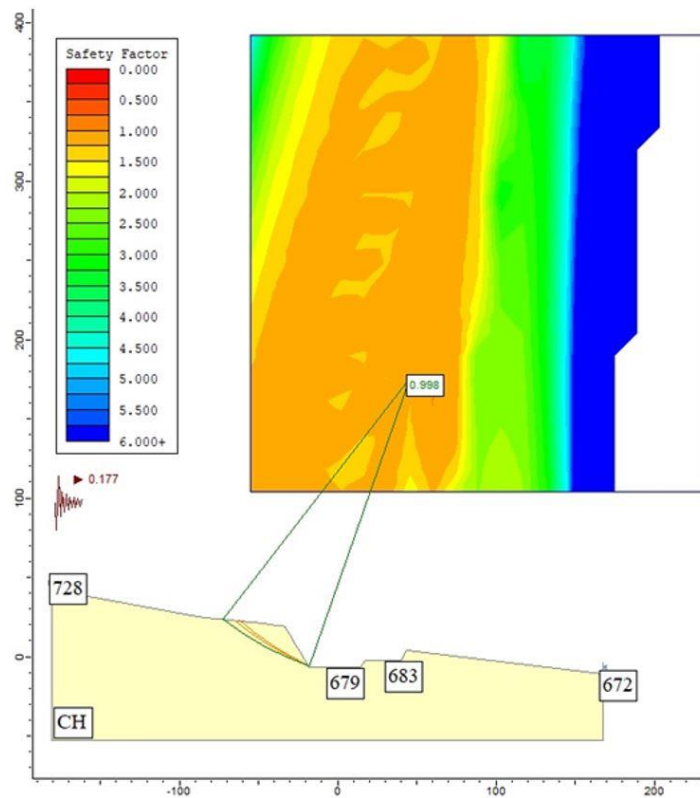


**Figure 5.** The minimum factor of safety (0.998) obtained for the dynamic condition for Line-I

Although the failure seems to have occurred after the excavation works started, considering the factor of safety values obtained as a result of the analyzes performed by considering the laboratory test data, it does not seem likely that any failure problem will arise under these conditions. However, there was a failure occurred in this line. In order for the stability to occur, changes in soil parameters (physical and mechanical) must have happened. This parameter change could only be possible by the precipitation that occurred before the failure in that region. Many researchers [29 - 35] revealed this with their studies in different regions. Since precipitation cannot be prevented in the region or anywhere, it is necessary to carry out studies to increase the factor of safety value.

The variation of the factor of safety value for the same conditions was examined by reconstructing a model for the benching process, which is one of the economical solutions that can be envisaged in order to increase the factor of safety value. For this purpose, 6V/6H (Bench Height/Bench Width) and 4 meters of step width were modeled and analyzed (Figure 6-7). The reason for choosing these values is to prevent possible sliding movements on slopes where mass movement does not occur, since, in the end, the entire working area where excavation works will be performed will actually be one slope. The analysis determined that the minimum safety factor of the slope in this state is 1.710 for the static situation and 1.063 for the dynamic situation. It turns out that the factor of safety of the slope in the dynamic case is close to the critical limit value. Since the dynamic conditions represent the most unfavorable conditions, the value of 1.000 to be obtained from here is sufficient for slope safety. According to TDBY [36], for the dynamic conditions safety coefficient should be greater than 1.10, but the  $S_{DS}$  (spectral acceleration coefficient) value is lower than the PGA (peak ground acceleration) value used in the analyzes; thus, 1.000 for the factor of safety value is applicable.

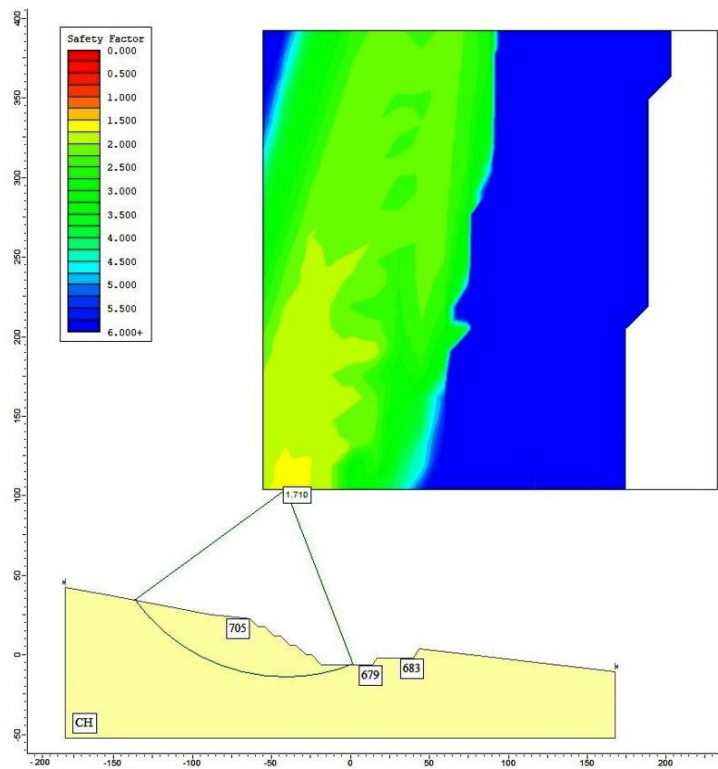


Figure 6. The minimum factor of safety (1.710) obtained for the static condition after the benching process of Line-I

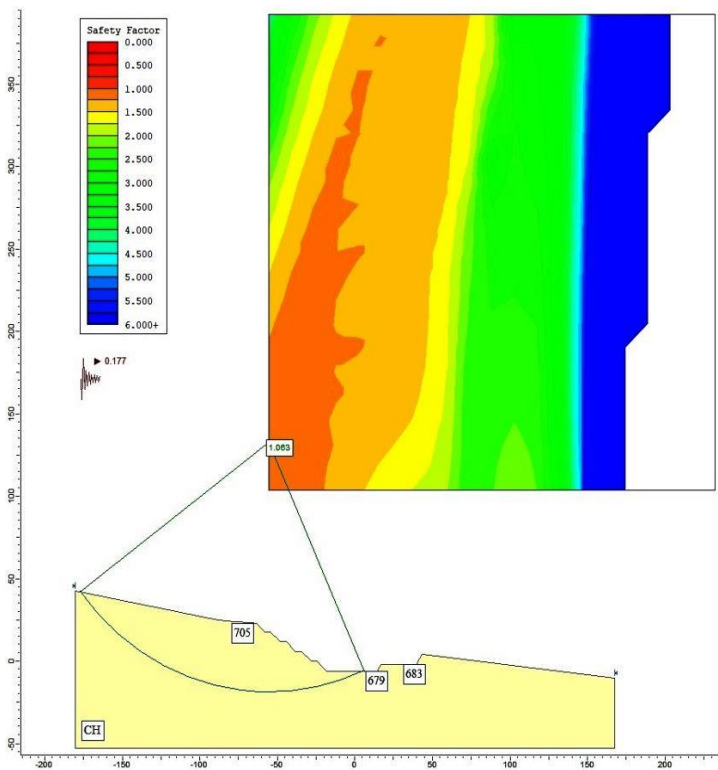


Figure 7. The minimum factor of safety (1.063) obtained for the dynamic condition after the benching process of Line-I.

### 3.2. Suggested Stabilization Method

Line 2 was created by considering the excavations to be carried out in accordance with the project within the slope surface with an average inclination of  $8.5^\circ$ . In the prepared cross-sections, the lower elevation of the slope was measured as 676 and the upper elevation as 716.5 m. The slope to be formed was considered as a single step and the lower elevation of this slope was given as 680 and the upper elevation as 706.50 by the survey engineers.

Line 3 was created by considering the excavations to be carried out in accordance with the project within the slope surface with an average inclination of  $6.5^\circ$ . In the prepared cross-sections, the lower elevation of the slope was measured as 673 and the upper elevation as 702 m.

For the two lines mentioned, analyzes were made considering the situations where the excavation works were finished. When all the excavation works are completed, since all three lines are part of a single slope, the slope arrangements were formed considering the 6V/6H (Bench Height/Bench Width) and 4 meters of step width. The factor of safety values obtained from the analysis are given in Table 1.

**Table 1.** Results of the analysis performed considering static/dynamic conditions for both benching process and no benching process

Lines	Static Conditions		Dynamic Conditions	
	No B.P.	B.P.	No B.P.	B.P.
Line 2	1.630	1.602	1.075	1.072
Line 3	1.623	2.078	1.176	1.426

\* B.P.: Benching process

### 4. Conclusions

Considering the static conditions analyzes performed with the data obtained from the laboratory experiments, failure occurred on the slope, although there should not have been any failure. When the analyzes carried out under the dynamic conditions checked, the factor of safety value decreases below 1,000. However, there was no earthquake activity at the time of the slope stability problem occurred. Based on the soil type (CH) forming the slopes, it is understood that there is a change in soil parameters (physical and mechanical) and a failure happened with the effect of precipitation in the region. During the study, other areas where the slope excavations were not completed in the project area were examined by two different lines (Line 2-3) and included in this study in order to avoid any failure problems might have occurred in the future. With the help of the analyzes performed within the scope of this study, models were formed for the slopes to be created in the future. Since all lines (Line 1,2 and 3) will belong to a single slope at the end of the project, all slope arrangements were modelled according to 6V/6H (Bench Height/Bench Width) and 4 meters of step width. For this reason, there has been a small decrease in the safety factor value for the dynamic and static conditions in Line II, but it is a negligible value. Apart from these precautions, covering the slope surface with shotcrete on such soils that are sensitive to water will contribute both in terms of water removal and stability. For situations or regions where water removal is thought to be ineffective, support structures such as retaining walls should be applied to the toe of the slopes formed.

### 5. Acknowledgement

The author would like to thank to Dr. Mesut Gor from Firat University, Faculty of Engineering, Department of Civil Engineering for his contribution to the article and the anonymous reviewers' comments to improve the paper.

### 6. Author Contribution Statement

In the study, Author 1 contributed (I) making the design and literature review, (ii) to checking the spelling and checking the article in terms of content.

## 7. Ethics Committee Approval and Conflict of Interest

There is no need for an ethics committee approval in the prepared article. There is no conflict of interest with any person/institution in the prepared article

## 8. References

- [1] Zhang J, Kuang M, Zhang Y, Feng T. "Evaluation and analysis of the causes of a landslide and treatment measures during the excavation of a tunnel through a soil-rock interface". *Eng. Fail. Anal.*, 130, 105784, 2021.
- [2] Guzzetti F, Carrara A, Cardinali M, Reichenbach P. "Landslide hazard evaluation: A review of current techniques and their application in a multi-scale study, Central Italy". *Geomorphology*, 31, 181-216, 1999.
- [3] García-Rodríguez MJ, Malpica JA, Benito B, Díaz M. "Susceptibility assessment of earthquake-triggered landslides in El Salvador using logistic regression". *Geomorphology*, 95, 172-191, 2008.
- [4] Rai, R. Factors affecting slope failure. Lecture Notes of Chapter 2, 2017.
- [5] Das BM. *Principles of Geotechnical Engineering*. Boston: Cengage Learning. 9nd ed. USA, 1994.
- [6] Akbulut İ, İlker ÇAM, Aksoy T, Çağlan D, Ölmez, T. "Açık ocaklarda şev duraysızlığı ve geriye dönük analizlere bir örnek: Afşin-Elbistan Kışlaköy açık kömür ocağı". *Maden Tetkik ve Arama Dergisi*, 147(147), 115-126, 2013.
- [7] Duncan JM, Wright SG. "*Soil strength and slope stability*". New York: John Wiley and Sons, Inc., 2005.
- [8] Zhang J, Tang WH, Zhang LM. "Efficient probabilistic back-analysis of slope stability model parameters". *Journal of Geotechnical and Geoenvironmental Engineering*, 136(1), 99-109, 2010.
- [9] Alemdag S, Kaya A, Karadag,M, Gurocak Z, Bulut F. "Utilization of the limit equilibrium and finite element methods for the stability analysis of the slope debris: an example of the Kalebasi District (NE Turkey)". *Journal of African Earth Sciences*, 106, 134-146, 2015.
- [10] Kaya A, Alemdağ S, Dağ S, Gürocak Z. "Stability assessment of high-steep cut slope debris on a landslide (Gumushane, NE Turkey)". *Bulletin of Engineering Geology and the Environment*, 75(1), 89-99, 2016.
- [11] Alemdağ S. "Toprak dolgulu barajlarda gövde duraylılığının limit denge ve sayısal analiz yöntemleri ile değerlendirilmesi: Türkiye'den bir atık barajı örneği". *Gümüşhane Üniversitesi Fen Bilimleri Enstitüsü Dergisi*, 6(2), 157-173, 2016.
- [12] Gör M. "Limit denge analizi (Bishop Yöntemi) ile kütle hareketinin mekanizması ve önlem yapısının analizi: Van ili örneği". *Gümüşhane Üniversitesi Fen Bilimleri Enstitüsü Dergisi*, 11(2), 597-608, 2021.
- [13] Taher NR, Gör M, Aksoy HS, Awlla HA. "Numerical investigation of the effect of slope angle and height on the stability of a slope composed of sandy soil". *Gümüşhane Üniversitesi Fen Bilimleri Enstitüsü Dergisi*, 12(2), 664-675, 2022.
- [14] Chowdhury R, Zhang S, Flentje P. "Reliability updating and geotechnical back-analysis". In *Advances in geotechnical engineering: The Skempton conference: Proceedings of a three day conference on advances in geotechnical engineering, organised by the Institution of Civil Engineers and held at the Royal Geographical Society*, 815-821, London: Thomas Telford Publishing, 2004.
- [15] Zhang LL, Zhang J, Zhang LM. Tang WH. "Back analysis of slope failure with markov chain monte carlo simulation". *Computers and Geotechnics*, 37(7-8), 905-912, 2010.
- [16] Akbaş B. "Probabilistic slope stability analysis using limit equilibrium, finite element and random finite element methods". Master Thesis, The Graduate School of Natural and Applied Sciences of Middle East Technical University, Ankara, 2015.
- [17] Zêzere JL, Trigo RM, Trigo IF. "Shallow and deep landslides induced by rainfall in the Lisbon region (Portugal): Assessment of relationships with the North Atlantic Oscillation". *Nat. Hazards Earth Syst. Sci.*, 5, 331-344, 2005.
- [18] Schmidt KM, Roering JJ, Stock JD, Dietrich WE. Montgomery DR, Schaub T. "The variability of root cohesion as an influence on shallow landslide susceptibility in the Oregon Coast Range". *Can. Geotech. J.*, 38, 995-1024, 2001.
- [19] Korup O. "Large landslides and their effect on sediment flux in South Westland, New Zealand". *Earth Surf. Process. Landf.*, 30, 305-323, 2005.
- [20] Larsen IJ, Montgomery DR, Korup O. "Landslide erosion controlled by hillslope material". *Nat. Geosci.*, 3, 247- 51, 2010.

- [21] Lin CW, Tseng CM, Tseng YH, Fei LY, Hsieh YC, Tarolli P. "Recognition of large scale deep-seated landslides in forest areas of Taiwan using high resolution topography". *J. Asian Earth Sci.*, 62, 389-400, 2013.
- [22] Rocscience Inc. Slide v. 06 Software. 439 University Ave. Ste. 780, Toronto, Canada, 2014.
- [23] Bishop AW. "The use of the slip circle in the stability analysis of slopes". *Geotechnique*, 5(1), 7-17, 1955.
- [24] Samtani NC, Nowatzki EA. Soils and Foundations Reference Manual Volume 1. U.S. Department of Transportation, Federal Highway Administration, Washington, D.C. 20590, 2006.
- [25] Bolgi TV. "Petrol Bölgesi seksiyon ölçmeleri AR/TPO/261 nolu saha ile Reşan- Dodan arası batısındaki sahanın strüktürel etüdüleri". TPAO Arama Grubu, Rapor,162, 52, 1961.
- [26] Kırathlıođlu E, Bolgi,T. "AR/TPO/609 nolu Kastel sahası ve civarının jeolojik etüdü. TPAO Arama Grubu". Rapor no: 220, 36, 1961.
- [27] Duran O, Şemşir D, Sezgin İ, Perinçek D. "Güneydođu Anadolu'da Midyat ve Silvan gruplarının stratigrafisi, sedimentolojisi ve petrol potansiyeli". TPJD Bülteni, Ankara c.1/2, 99-126, 1988.
- [28] Duran O, Şemşir D, Sezgin L, Perinçek D. "Güneydođu Anadolu'da Midyat Silvan Gruplarının stratigrafisi, sedimantolojisi ve paleocografyası, paleontolojisi, jeoloji tarihi, rezervuar ve diyajenez özellikleri ve olası petrol potansiyeli". TPAO Araştırma Merkezi, Rapor No.2563, 1989.
- [29] Lim TT, Rahardjo H, Chang MF, Fredlund DG. "Effect of rainfall on matric suctions in a residual soil slope". *Can. Geotech. J.*, 33, 618–628, 1996.
- [30] Vanapalli SK, Fredlund DG, Pufahl DE, Clifton AW. "Model for the prediction of shear strength with respect to soil suction". *Can. Geotech. J.* 33, 379–392, 1996.
- [31] Godt JW, Baum RL, Savage WZ, Salciarini D, Schulz WH, Harp EL. "Transient deterministic shallow landslide modelling: requirements for susceptibility and hazard assessment in a GIS framework". *Eng. Geol.* 102, 214–226, 2008a.
- [32] Godt JW, Schulz WH, Baum RL. "Savage,W.Z. Modelling rainfall conditions for shallow landsliding in Seattle, Washington". In: Baum, R.L., Godt, J.W., High land, L.M.(Eds.), Landslides and Engineering Geology of the Seattle,Washington, area. *Geol Soc Am Rev Eng Geol* 20, 137–152, 2008b.
- [33] Godt JW, Baum RL, Lu N. "Landsliding in partially saturated materials". *Geophys. Res. Lett.* 36, 2009.
- [34] Baum RL, Godt JW, Savage WZ. "Estimating the timing and location of shallow rainfall-induced landslides using a model for transient, unsaturated infiltration". *J. Geophys. Res.*, 2010.
- [35] Lu N, Godt JW. "Hillslope hydrology and stability". *Cambridge University Press*, Cambridge, U.K, 2013.
- [36] TBDY, Türkiye Bina Deprem Yönetmeliđi. T.C. Resmi Gazete; 30364, 2018.